The Thesis Committee for Derek Andrews Tinker

Certifies that this is the approved version of the following thesis:

Pore-Scale Permeability Prediction using Critical Path Analysis

APPROVED BY

SUPERVISING COMMITTEE:

Supervisor: _____

Hugh Daigle

_____

Mukul M. Sharma

Pore-Scale Permeability Prediction using Critical Path Analysis

by

Derek Andrews Tinker, B.S.

Thesis

Presented to the Faculty of the Graduate School of

The University of Texas at Austin

in Partial Fulfillment

of the Requirements

for the Degree of

Master of Science in Engineering

The University of Texas at Austin

August 2016

Acknowledgements

In the six months of my graduate degree, oil prices tumbled from just over 100 dollars a barrel in August ’14 to 47 dollars in January of ’15. The shock of this drop was felt throughout the industry and academia was not immune. Completing a Masters of Science degree in this climate has proven to be an immensely challenging, but equally rewarding experience. The opportunity has helped me broaden my understanding and appreciation for the science of engineering and gain deeper insight into petroleum engineering and petrophysics.

I would first like to thank my advisor, Dr. Hugh Daigle. Despite being stretched thin with a large lab group, he took me on in a time of need and challenged me to apply to be a Statoil Fellow. His relaxed nature and positive outlook are contagious and I credit him with helping me understand the importance of learning to learn. I would also like to thank Dr. Mukul Sharma for teaching me the fundamentals of Hydraulic Fracturing and serving as my second reader.

I am also grateful to Glen Baum, who helped me to install and find ways to devise experimental equipment. My sincere gratitude also goes out to Frankie Hart and Amy Douglas Stewart for their administrative support throughout the entire process. I would also like to thank all the faculty and staff members at Petroleum Geosystems Engineering Department for helping to make my graduate experience a fulfilling one and for helping to prepare me for a career in Petroleum Engineering.

Finally, I would like to thank my family and friends for their support and understanding throughout this process.

Abstract

Pore-Scale Permeability Prediction using Critical Path Analysis

Derek Andrews Tinker, M.S.E.

The University of Texas at Austin, 2016

Supervisor: Hugh Daigle

Using the principles set forth in percolation theory and critical path analysis (CPA), this thesis presents a method for constraining parameterized values of critical pore size and a cumulative volumetric density function using the shape and scale of accessibility functions and a mercury intrusion capillary pressure (MICP) data set. Constraints can be made without an independent pore size distribution measurement. These parameters can be combined with the percolation threshold corrected for finite sample size and electrical formation factor to determine permeability and to approximate pore size distribution. The analysis uses predetermined permeability, porosity, and formation factor values in Berea Sandstone and Racine Dolomite core samples to initially quantify parametrization values. The analysis also compares two methods of deriving critical pore size using the Washburn equation and using parameterized values. The thesis also takes an initial look at applying the method to different methods for parameterizing the pore size volumetric probability density function; first using a pore solid fractal (PSF) model known to be appropriate in natural porous media and then using a truncated power law (TPL) distribution for comparison.

Table of Contents

List of Tables

List of Figures

CHAPTER 1: INTRODUCTION

An important concept within the petrophysics and broader reservoir characterization community is understanding fluid flow through porous media, and specifically quantifying permeability. Numerous attempts over the last ninety years have been made to define characteristic rock properties in order to better understand and model the ease of flow through reservoir rocks. Historically, the first approaches were based off work done by Carman and Kozeny, who expressed permeability as a function of hydraulic radius (pore volume divided by pore surface area) and other macroscopic properties (Katz & Thompson, 1986; P.C. Carman, 1956). Attempts were made to define hydraulic radius as a characteristic length and justify this on the basis of an effective medium model. According to Katz and Thompson (1986), these attempts fail because they attempt to relate macroscopic geometric properties with transport properties and they do not distinguish the physical significance and sensitivity of the scale of length in permeability prediction. Katz and Thompson (1986) helped to define a critical pore size r_c (the smallest pore space within a sample-spanning, connected cluster of pores) as an important parameter with regard to permeability prediction. In a recent manuscript, Daigle (2016a) points out that there are in fact two fundamental length scales in describing transport through the pore space: the critical pore size r_c and the size of the medium. Considering both can result in greater accuracy when predicting permeability. This thesis expands on these findings by (1) presenting a method for defining parameters for future, lithology-specific permeability prediction using only mercury intrusion capillary pressure (MICP) data and knowledge of electrical formation factor that does not require and independent measurement of the pore size distribution, (2) highlighting the need for a geometry dependent coefficient in

permeability prediction models, and (3) observing clear, numerical differences between proposed methods for determining critical pore size r_c.

1.1 Introduction to Critical Path Analysis and Percolation Theory

1.1.1 Critical Path Analysis

The basic principle of CPA is that in a highly heterogeneous medium, the majority of flow occurs through high-conductance pathways. Flow through these pathways is limited by the least-conductive sections or "bottlenecks". Ultimately, the size and frequency of the bottlenecks greatly influence the macroscopic transport properties. A number of researchers (Friedman & Seaton, 1998; Hunt, 2001; Skaggs, 2011) have noted the analogous properties displayed by electrical and hydraulic conduction. According to these findings, conduction of both types occurs through higher-conductivity pore sizes in the medium. With *f(r)* representing the volumetric probability density function and r_c as a critical pore size, the percolation threshold p_c for an infinite medium, may be defined as

$$p_c = \int_{r_c}^{\infty} f_r(r)dr \tag{1.1}$$

The critical pore size represents the smallest pathway restricting flow through a sample-spanning, connected cluster of pores.

CPA was initially utilized to analyze conduction in disordered systems such as amorphous semiconductors. The success of CPA in semiconductors does not necessarily imply that it is applicable to fluid flow in porous media due to potential differences in the nature of flow, however, there have been various attempts made to verify a relationship between the two flow types. According to Skaggs (2011), a number of past applications of

CPA to pore network models have produced good matches when compared to experimental results, while other studies raise questions about the applicability of CPA to porous media. Skaggs (2011) goes on to highlight a few fundamental questions with the assumptions on which CPA is built.

1. Can the localized transport through the largest pores be used to accurately predict transport in porous media?
2. CPA assumes that in the limit of a very broad pore size distribution, the conductance through the critical pore size r_c controls the conductance of the medium. Does this correlation arise from a coincidental correlation of r_c with other length scales?

Daigle (2016a) uses a set of experimental data to confirm the applicability of CPA for predicting transport in porous media and explains that both r_c and the length of medium are fundamental length scales for transport in porous media, despite the correlation between r_c and other length scales.

1.1.2 Percolation Theory

The natural language for describing connectivity-related phenomena is percolation theory (Broadbent & Hammersley, 1957). When applied to porous media, percolation theory describes the behavior of connected clusters of pores in a random system. Commonly, percolation is modeled using a randomly distributed system of bonds within square or cubic lattices. The square lattice shown in Fig. 1(a) consists of an array of sites, each of which is joined with its neighbors by bonds. These bonds are considered to have two possible states: occupied and unoccupied, represented with a line or space in the figure respectively (Seaton, 1991). The presence of a bond within the square or cubic lattice can be associated with a probability p, calculated by dividing the number of occupied bonds by

the total number of bonds in the system. As p is increased, the number of bonds in the system will also increase, forming larger clusters of bonds, illustrating the phenomenon known as percolation. On an infinite lattice, the formation of a spanning cluster occurs at a specific value of p known as the percolation threshold, p_c, as shown in the highlighted bond in Figure 1.1(b). Various authors have outlined the significance of the percolation threshold in relation to permeability by relating it to the critical pore size r_c as in Eq. 1 and the formation factor F. The percolation of bonds across a lattice can be physically analogized by progression of mercury through a core sample at increasing pressures that occurs in a mercury intrusion capillary pressure (MICP) measurement.

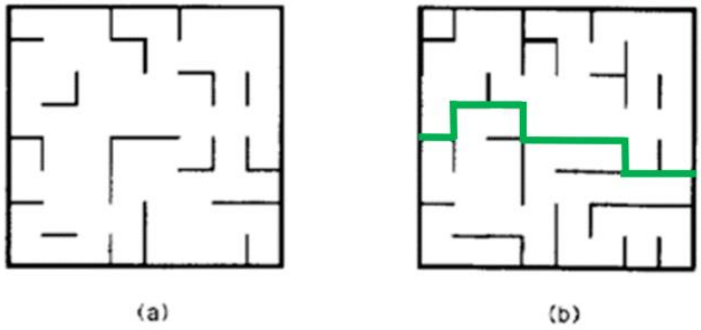

Figure 1.1: Square lattices (a) below the percolation threshold and (b) at the percolation threshold (Seaton, 1991).

1.2 Research Objectives

The overall goal of this thesis was to provide further insight into the calculation of permeability in highly heterogeneous media using Critical Path Analysis. More specifically, there have been recent models that suggest that the fluid transport through porous media is not limited to one dominant fundamental length scale (critical pore size)

and that prediction can be refined by including both critical pore size and the length of the medium.

Building upon these findings, a method for creating prediction parameters to make it possible to approximate lithology-specific permeability using only Mercury Intrusion Capillary Pressure (MICP) results and a knowledge of formation factor was imagined and initiated in Berea Sandstone and Racine Dolomite. This method was applied to two different approaches for parameterizing a pore-size distribution: a pore-solid fractal model and a truncated power law distribution. Additionally, the results were used to help quantify a pore geometry dependent coefficient necessary for accurate permeability prediction. Finally, results were studied to identify the numerical difference between proposed methods for determining critical pore size.

1.3 Description of Chapters

The second chapter provides theoretical support for the methods underpinning the predictive model. The third chapter discusses relevant laboratory results and outlines methodology used in the predictive model. The fourth chapter discusses the results of the experiments performed. The final chapter discusses the conclusions reached from the experiments and suggestions for future work to refine accuracy of the parameters presented in the results.

CHAPTER 2: THEORY AND ANALYTICAL BACKGROUND

2.1 PARAMETERIZING THE PORE SIZE DISTRIBUTION

In investigations of CPA, authors have used several different methods of parameterizing the pore size distribution. Skaggs (2011), Le Doussal (1989b), and others use a log-uniform distribution because it is typically a good fit for conductance distribution in semiconductors, However, a number of authors such as Hunt (2001), Hunt and Gee (2002), and Sahimi (1993) present evidence that pore sizes in natural porous media tend to follow fractal scaling with finite upper and lower bounds and that fractal parameterization can allow for more successful prediction of transport properties. Bird et al. (2000) and Perrier et al. (1999) summarize the use of a particular fractal model, the pore-solid fractal (PSF) model, whose parameters advantageously all have a physical interpretation and results in a type of power-law distribution. I used the PSF model to define the parameters relevant to this thesis. I additionally generalize the method to allow for different pore size distribution parameterizations to be used.

Given a parameterized volumetric probability density function, a number of calculations can be made to obtain the cumulative probability density function for pore sizes $V(<r)$, percolation threshold, and critical pore size. The cumulative probability density function for pore sizes $V(<r)$ may be obtained by integrating the volumetric probability density function $f_g(r)$ between the minimum pore size r_{min} and any pore size such that $r_{min} \leq r \leq r_{max}$. The percolation threshold may be determined by carrying out the integration of the probability density function $f_g(r)$ presented in Eq. 1.1. The resulting equation can then be rearranged to obtain critical pore size r_c.

In the following sub-sections I will parameterize the pore size volumetric probability density functions developed from a truncated power-law distributions and using

the PSF model. This will ultimately give a basis for the numerical comparison of two methods used to parameterize the pore-size distribution.

2.1.1 Pore-Solid Fractal Model

The PSF model considers the porous medium to be composed of three components: pores, solids, and volume in which the fractal generator is replicated iteratively. In three dimensions, the volumetric probability density function can be expressed as

$$f_r(r) = \frac{\beta}{\phi}\frac{3-D}{r_{max}^{3-D}} r^{2-D} \tag{1.2}$$

where ϕ is porosity, D is the fractal dimension, r_{max} is the largest pore-size in the medium, and β is the ratio of the pore volume to the sum of the pore and solid volumes in the fractal model. In the model, β does not include the volume in which the fractal generator is replicated, signifying that $\beta \geq \phi$. The cumulative probability density function for pore sizes $V(<r)$ can be parametrized as follows:

$$V(<r) = \frac{\beta}{\phi}\frac{3-D}{r_{max}^{3-D}}\int_{r_{min}}^{r} r_i^{2-D} dr_i = \frac{\beta}{\phi}\left[\left(\frac{r}{r_{max}}\right)^{3-D} - \left(\frac{r_{min}}{r_{max}}\right)^{3-D}\right] \tag{1.3}$$

where r_i is the variable of integration. The percolation threshold p_c can be expressed as follows

$$p_c = \frac{\beta}{\phi}\frac{3-D}{r_{max}^{3-D}}\int_{r_c}^{r_{max}} r_i^{2-D} dr_i = \frac{\beta}{\phi}\left[1 - \left(\frac{r_c}{r_{max}}\right)^{3-D}\right] \tag{1.4}$$

This can be rearranged to obtain critical pore size r_c

$$r_c = r_{max}\left(1 - \frac{\phi p_c}{\beta}\right)^{\frac{1}{3-D}} \tag{1.5}$$

2.1.2 Truncated Power-law Distribution

The volumetric density function can be generically modeled as a truncated power law pore-size distribution such that

$$f_r(r) = \frac{A_r}{2} r^{-\alpha-1} \tag{1.6}$$

where α is the distribution shape parameter, $r_{min} \leq r \leq r_{max}$, and $A_r = {}^{\alpha}/_{(r_{min}^{-\alpha} - r_{max}^{-\alpha})}$ is the normalization constant ($\alpha \neq 0$). The cumulative probability density function for pore sizes $V(< r)$ can be parametrized as follows

$$V(< r) = \frac{\alpha}{(r_{min}^{-\alpha} - r_{max}^{-\alpha})} \int_{r_{min}}^{r} r_i^{-\alpha-1} dr_i = \frac{(r_{min}^{-\alpha} - r^{-\alpha})}{(r_{min}^{-\alpha} - r_{max}^{-\alpha})} \tag{1.7}$$

where α is the distribution shape parameter and r_i is the variable of integration. The percolation threshold p_c can be expressed as follows

$$p_c = \frac{\alpha}{(r_{min}^{-\alpha} - r_{max}^{-\alpha})} \int_{r_c}^{r_{max}} r_i^{-\alpha-1} dr_i = \frac{(r_c^{-\alpha} - r_{max}^{-\alpha})}{(r_{min}^{-\alpha} - r_{max}^{-\alpha})} \tag{1.8}$$

This can be rearranged to obtain critical pore size r_c

$$r_c = [(1 - p_c) r_{max}^{-\alpha} + p_c r_{min}^{-\alpha}]^{-\frac{1}{\alpha}} \tag{1.9}$$

2.2 PORE NETWORK MODEL

CPA was originally developed to analyze local conductance as a function of randomly distributed system parameters that are uniformly distributed in semiconductors. Taking W as the breadth of the pore size distribution, a measure of the degree of heterogeneity in the system, and assuming $W \gg 1$, the local conductances g for both hydraulic and electric systems in which conductances are exponential functions of random

system parameters which are uniformly distributed will follow a log-uniform distribution such that the probability density function for microscale conductance is

$$f_g(g) = \frac{1}{Wg} \tag{1.10}$$

CPA can yield an approximation of the macroscopic conductivity for sufficiently large W (i.e. $W \geq 5$) such that the macroscopic conductivity Σ, can be represented as

$$\Sigma = CW^{-y} g_c \tag{1.11}$$

where C is a system dependent constant and y is a prefactor exponent (Skaggs, 2003). The prefactor exponent is not clearly defined for all systems, but is generally accepted to depend solely on the spatial dimension of the system (Skaggs, 2011). Le Doussal (1989) proposed that in the limit $W \to \infty$, the exponent can be calculated using the form

$$y = (d-2)\nu \tag{1.12}$$

where d is the spatial dimension (d=3 for a 3-dimensional system) and ν is a fundamental length of percolation theory ($\nu = 0.88$ for $d = 3$; $\nu = 4/3$ for $d = 2$) (Sahimi, 1993). This hypothesis has been confirmed for 2D systems, but the value of the correlation length for 3D systems must be further studied (Le Doussal, 1989a; Skaggs, 2003). One goal of this thesis is to further the understanding of the effect of the prefactor exponent within a strongly heterogeneous porous medium by comparing laboratory results with the predictive results given by the CPA model.

The conductance g, of a pore in a network of liquid-saturated pores arranged on a regular lattice with fixed pore length l_o, is given by

$$g = g_o \delta^m \tag{1.13}$$

where constants g_o and m depend on pore geometry and the nature of the transport and δ is a characteristic length. Characteristic length defines pore radius for cylindrical pores and pore width for slit-shaped pores, but can be generalized as "pore-size" (Skaggs, 2011). Allowing for a varied nature of transport allows g to refer to hydraulic or electrical conductance. Assuming that g is uncorrelated in space, that the slit-shaped pores have a breadth b much wider than the width δ, taking μ to be the dynamic viscosity, and $C = {}^{l}/_{r} = {}^{2l}/_{\delta}$, the constants in Eq. 2.12 can be defined as in Tables 2.1 and 2.2. Additionally, it is necessary to assume that the surface of the pore is nonconducting to use Eq. 2.12 for electrical conductance.

Type of Conductance	**Type of Flow**	***m***	***g_o***	***g (Eq. 2.12)***
Electrical	Electrical Current	2	${}^{\pi\rho_w}/_{4l_o}$	$g_e = {}^{\pi r\rho_w}/_{C}$
Hydraulic	Viscous	4	${}^{\pi}/_{128\mu l_o}$	$g_h = {}^{\pi r^3}/_{8C\mu}$

Table 2.1: Constants used to define local conductance for electrical and hydraulic current in cylindrical pores

Type of Conductance	Type of Flow	*m*	g_o	*g (Eq. 2.12)*
Electrical	Electrical Current	1	$\rho_w b / l_o$	$g_e = 2\rho_w b / C$
Hydraulic	Viscous	3	$b / 12\mu l_o$	$g_h = 2br^2 / 3C\mu$

Table 2.2: Constants used to define local conductance for electrical and hydraulic current in slit-shaped pores

2.3 CRITICAL PATH ANALYSIS

The relationship between critical conductance and macroscopic hydraulic or electrical conductivity is central to the calculation of permeability in highly heterogeneous media using CPA. Although most authors agree that the bottleneck conductance with a critical value plays a significant role in limiting transport, different conductivity calculations are possible depending on assumptions made about the frequency of the bottlenecks and how their separation varies with the degree of heterogeneity (Skaggs, 2011). Practically, formulating the ratio of the hydraulic and electrical conductivities of the same pore network helps to eliminate many of the system constants. Two methods of calculating these conductivities, based on different generalized assumptions are considered below.

2.3.1 Tyč and Halperin Method

Tyč and Halperin (1989), Skaggs (2011), Le Doussal (1989b), and others related the critical conductances g_c with macroscopic conductances utilizing a generalization of Eq. (2.10)

$$\Sigma = C g_c \left[g_c f_g(g_c) \right]^y \tag{1.14}$$

According to Tyč and Halperin (1989), the estimation is applicable to hydraulic conductivity or bulk electrical conductivity given that f_g is broad, which occurs when $g_c f_g(g_c) \ll 1$ and $g f_g(g)$ is slowly varying in a large neighborhood about g_c.

2.3.2 Friedman and Seaton Method

According to Friedman and Seaton (1989) and Hunt (2001), the average spatial separation of critical conductances must be equal to the average spatial separation of conductive pathways in pore radii larger than the critical pore size ($r > r_c$). This condition may be met in semiconductors, but not for conduction in natural porous media. It follows that in natural porous media

$$\Sigma = g_c = g_o(2r_c)^m \tag{1.15}$$

where values for g_0 and m depend on pore geometry and the nature of the transport can be found in Tables 2.1 and 2.2.

2.4 Permeability From Critical Path Analysis

Formulating the ratio of the hydraulic and electrical conductivities of the same pore network is practically useful to eliminate many of the system dependent constants present in Eqs. 2.13 and 2.14. Taking m_H, m_E, $g_{0,H}$, and $g_{0,E}$ as the constants defined in Tables 2.1 and 2.2, the following expression can be obtained for both the power law and lognormal distributions developed using the Tyč and Halperin Method:

$$\frac{\Sigma_H}{\Sigma_E} = \frac{\Sigma(m_H, g_{0,H})}{\Sigma(m_E, g_{0,E})} = \frac{g_{0,H}}{g_{0,E}}\left(\frac{m_H}{m_E}\right)^{-y}(2r_c)^{m_H - m_E} \tag{1.16}$$

The same ratio can be developed using the Friedman and Seaton method as follows:

$$\frac{\Sigma_H}{\Sigma_E} = \frac{\Sigma(m_H, g_{0,H})}{\Sigma(m_E, g_{0,E})} = \frac{g_{0,H}}{g_{0,E}}(2r_c)^{m_H - m_E} \tag{1.17}$$

In the absence of surface conductivity, the ratio of electrical conductivities ρ_b/ρ_w will equal $1/F$ where F is Archie's formation resistivity factor (Archie, 1942). Applying this reduction and assuming that fluid permeability k is equal to $\Sigma_H \mu$, $\rho_b = \Sigma_E$ is the bulk electrical conductivity, ρ_w is the electrical conductivity of the saturating fluid, and r_c is the critical pore radius, permeability for pore cylindrical and slit-shaped pores using the two methods can be defined as follows

Tyč and Halperin Method

Cylindrical Pores:

$$k = \frac{2^{-y}}{8}\frac{\rho_b}{\rho_w}r_c^2 = \frac{2^{-y}}{8}\frac{r_c^2}{F} \tag{1.18}$$

Slit-Shaped Pores:

$$k = \frac{3^{-y}}{3}\frac{\rho_b}{\rho_w}r_c^2 = \frac{3^{-y}}{3}\frac{r_c^2}{F} \tag{1.19}$$

Friedman and Seaton Method

Cylindrical Pores:

$$k = \frac{r_c^2}{8}\frac{\rho_b}{\rho_w} = \frac{r_c^2}{8F} \tag{1.20}$$

Slit-Shaped Pores:

$$k = \frac{r_c^2}{3}\frac{\rho_b}{\rho_w} = \frac{r_c^2}{8F} \tag{1.21}$$

2.5 Analytical Methods Background

Background information for the variety of applicable laboratory tests to acquire pore size distribution, formation factor, and critical pore size are presented in the following sections.

2.5.1 Resistivity Measurements

In the absence of surface conductivity, Ghanbarian et al. (2014) combined percolation theory (valid near the percolation threshold) with effective medium theories (valid near $p = 1$) in a piecewise function to express F as follows

$$\frac{1}{F} = \begin{cases} \dfrac{\left(\phi(1-p_c)\right)^2}{(1-\phi p_c)(\phi_x - \phi p_c)} & \phi p_c < \phi < \phi_x \\ \dfrac{1-\phi p_c}{\phi(1-p_c)} & \phi_x < \phi < 1 \end{cases} \tag{1.22}$$

where ϕ_x is the crossover porosity at which the scaling of electrical conductivity crosses from percolation theory to effective medium theory. Ghanbarian et al. (2014) analyzed 405 sets of porosity and formation factor data and found that values can vary from $0.4 < \phi_x < 1$, indicating that the crossover porosity in the porosity-dependent formation factor model is not universal.

The equation holds for porosities such that $\phi p_c < \phi \leq 1$ as long as p_c is not very small. The exponent in Eq. 2.21 is known to be universal as long as the pore size

distribution is not too broad and the properties of the porous medium do not exhibit long-range correlation. Long-range correlations in borehole logs have been shown to result in exponents less than 2. All of these conditions are known to be met in laboratory samples of sedimentary rocks, making Eq. 2.21 appropriate for permeability approximation in sedimentary samples.

However, one major issue with calculating the formation factor using Eq. 2.21 is that the crossover porosity ϕ_x has been known to vary from 0.26 to 1 in various samples and has been shown to vary even within samples of the same lithology (Ghanbarian et al., 2014). Daigle (2016a) and Daigle et al. (2015) circumvent this variance by assuming that $\phi_x = 1$, implying that universal scaling of the percolation theory would be valid from the percolation threshold all the way to $\phi = 1$. The average sandstone sample tested by Ghanbarian et al. (2014) was closer to 0.75, suggesting it might not be appropriate to use a crossover porosity equal to 1 for permeability prediction in Berea and Racine samples. Since detailed information, such as capillary pressure data or 3-D images, were not available, Ghanbarian et al. (2014) calculated various crossover porosity values under the assumption that $p_c = 0.1\phi$. This assumption however is probably not universally valid. Thus, until further experimental data determining crossover porosity in specific lithologies becomes available, it is more appropriate to measure formation factor separately. A small section in the results is devoted to using determined percolation threshold and formation factor values to calculate ϕ_x for the lithologies studied.

A common method for measuring formation factor is to manually test the bulk resistivity of the appropriate cores R_b and the resistivity of the saturating fluid R_w. Since $R_i = {}^{1}/_{\rho_i}$, the formation factor can be determined via the general form of Archie's law for rocks devoid of clay as $F = \rho_b/\rho_w = R_w/R_b$ (Archie, 1942).The resistivity of the

saturating fluid R_w can be determined for the specific NaCl concentration of the saturating fluid and temperature of the testing environment using the chart shown in Figure A3.2.

The bulk resistivity R_b of the core can be determined using a resistivity core holder. During a core holder measurement, it is necessary to first dry, evacuate, and saturated the core sample with a NaCl brine solution. Two six millimeter measuring electrode probes are positioned on the outer surface of each end of the core sample, flush with the curvature. The distance between the two electrodes is defined as the effective length L_{eff}. Using the core holder, a confining pressure is applied to either end and a current is passed between two confining electrodes positioned on opposite ends of the core sample. Voltage V_1 is measured across a 1kΩ resistor and voltage V_2 is measured across the pair of electrodes in the core. The generated current is constant and can be represented using Ohm's law as $I = {V_1}/{1k\Omega} = {V_2}/{r_o}$ where r_o is the resistance across the effective length between the two measuring electrodes. Rearranging this equation yields

$$r_o = \frac{1000V_2}{V_1} \tag{1.23}$$

Given a core area defined by $A = \pi r^2$, resistivity of the fully saturated core R_b can be determined as

$$R_b = \frac{r_o A}{L_{eff}} \tag{1.24}$$

The measured values of bulk resistivity R_b and brine resistivity R_w can be used to determine formation factor $F = R_w/R_b$.

2.5.2 Mercury Intrusion Capillary Pressure (MICP)

Due to its simplicity and utility, mercury injection capillary pressure (MICP) has become a widely used method for modeling pore size and volume distribution. Additionally, mercury is a nonwetting fluid for most solids, which makes the capillary pressure curve derived from mercury injection a well-suited model for probing the pore structure of porous media. Applying the CPA model for the ratio of the hydraulic and electrical conductivities does not require any knowledge of the underlying pore size distribution, only the value of the critical pore size r_c. Fortunately, this value can be derived from a pore volume distribution, which does not assume a model for the pore geometry such as a bundle of capillary tubes or slit-shaped pores.

During an MICP measurement, a sample is dried and evacuated, then immersed in mercury. The pressure of the mercury is gradually increased causing mercury to intrude into the sample. Capillary pressure, P_c, is defined as the pressure discontinuity between two immiscible fluids which is dependent on the curvature of the interface separating them. When mercury is injected into the porous medium at a low pressure, mercury will only enter those pores having pore throat radii equal to or greater than the radius given by the Washburn equation:

$$P_c = \frac{2\sigma|cos\theta|}{r} \tag{1.25}$$

where r is the pore throat radius, σ is surface tension, θ is contact angle (Purcell, 1949). Increasing the capillary pressure will allow the mercury to invade pores with smaller pore throat sizes. At a high enough capillary pressure, all the interconnected pores in the medium

will be invaded by the mercury. Monitoring the cumulative volume of mercury injected versus the capillary pressure or pore throat radii can yield a pore volume distribution.

Katz and Thompson determined critical pore size on rock samples using mercury intrusion measurements. By simultaneously measuring the electrical resistance of the sample, they demonstrate that the inflection point of a plot of volume fraction versus pore pressure corresponds to the point at which the mercury first forms a cluster spanning the sample, or the threshold pressure. Utilizing the Washburn equation, they conclude that the pore radii included in the infinite cluster satisfy the relation

$$r_c = \frac{-2\sigma|cos\theta|}{P_t} \tag{1.26}$$

where σ is surface tension, θ is contact angle, and P_t is defined as the threshold pressure for the formation of the infinite cluster (Katz & Thompson, 1986, 1987).

The mercury injection process can be related to percolation theory as shown in Figure 2.1. As mercury pressure increases from 0, pores with lower entry pressures than the mercury pressure that are connected to the exterior of the sample are filled with mercury. These pores are represented by lines in the simple two-dimensional pore system representations. The percolation threshold is marked by a vertical dashed line, and denotes the point when enough pores have been filled with mercury to form a sample-spanning cluster of filled pores. Above the percolation threshold, more of the pores are filled creating numerous sample-spanning clusters (Katz & Thompson, 1986).

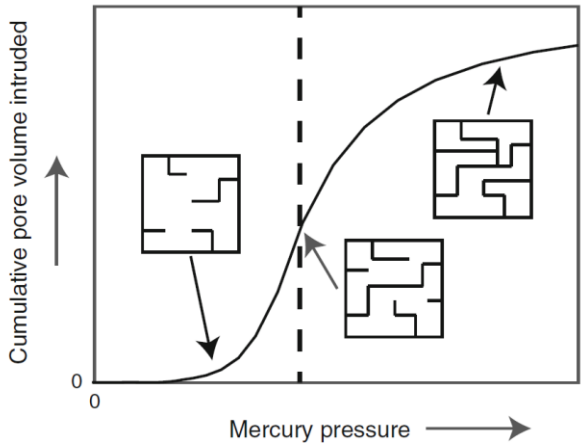

Figure 2.1: Idealized representation of percolation during a mercury intrusion measurement (Daigle & Johnson, 2016).

2.5.3 Correction for finite scaling

Percolation theory and CPA assume an infinite lattice. The fact that physical samples are not infinite in size can cause a scale dependence of the permeability measurement itself as well as a scale dependence of the apparent percolation threshold (Daigle, 2016a). For the first effect, the permeability can be corrected using a factor of $1 + [\lambda/x]^3$ where x is the smallest relevant edge length in the core samples measured and λ is the average separation between pores (Hunt, 1998) and can be approximated using $\lambda \approx r_{max}$ (Hunt, 2001). Thus, using permeability measurements made on Berea and Racine cylindrical core plugs 2.54 cm in diameter and 5.08 cm in length with a value of $r_{max} = 30\ \mu m$, x can be approximated as 2.54 cm since that is the smallest relevant dimension (Daigle, 2016a). Using these values, a correction factor of $(1 + [0.003/2.54]^3) = 1 + 2 \times 10^{-9}$ can be approximated. Thus, the corrected values would only differ from infinite media by 2 parts in one billion, indicating that no finite size correction is necessary for permeability measurements.

Correcting the percolation threshold due to the finite size of the core has a more measureable effect. Typically, the interpretation of a drainage capillary pressure curve is obtained by assuming the porous medium to consist of a bundle of capillary tubes, implying that all pores are equally accessible to the invading mercury. Significant errors arise in finite samples because the capillary tube model underestimates the fraction of larger pores and overestimates the fraction of smaller pores. Therefore, it is necessary to account for the discrepancy in accessibility due to the capillary tube model (Mishra & Sharma, 1988).

The scale-dependence of the percolation threshold, which is a function of sample size and pore length, can be mapped as a function of critical pore size and sample size assuming a self-similar pore system. Daigle (2016a) shows that the correction for this scale dependence is a function of the breadth of the pore size distribution and pore system heterogeneity. More specifically, the length scale separating heterogeneities along the percolating network, or correlation length, is assumed to be smaller than the linear size L of the medium in percolation theory. L is often presented in multiples of the critical pore length of the system. When the linear size L of the medium is smaller than the correlation length, the apparent percolation threshold obtained using laboratory results will be smaller than the true percolation threshold for an infinite sample size. A correction factor of $L^{-1/\nu}$, where $\nu = 0.88$ in three dimensions, is used to scale the laboratory measurement of percolation threshold (Sahimi, 1993). In practice, if $p_c(L)$ is the percolation threshold of a medium of linear size L and a is a constant that varies based on the sample, then the corrected percolation threshold can be expressed as

$$p_c = aL^{-\frac{1}{\nu}} + p_c(L) \tag{1.27}$$

Using results presented by Daigle (2016a), $a = 2.238$ for Berea and Racine samples. Prediction using Eqs. 2.17 – 2.20 requires a knowledge of pore geometry, which requires extra equipment or potentially inaccurate assumptions to be made. By introducing a single constant c in place of the leading coefficients Eq. 2.17 and Eq. 2.18 so that $2^{-y}/8 \leq c \leq 3^{-y}/3$, the knowledge of pore geometry is no longer necessary. In three dimensions, $y = \upsilon(d-2) = \upsilon = 0.88$, and therefore Eq. 2.17 and Eq. 2.18 can be reduced to

$$k = \frac{cr_c^2}{F} \tag{1.28}$$

The reduction using the Friedman and Seaton method (Eq. 2.19 – 2.20) is the same, with the constant *c* assumed to be between 1/8 and 1/3.

One method for determining the finite linear medium size L is outlined in Daigle (2016a)and is developed using a modified version of the procedure used by Liu et al. (1992, 1993) and Daigle and Johnson (2016). In this procedure, a relationship of probabilities presented in percolation theory is envisioned in terms of an MICP measurement and modified to collapse onto a family of type curves solely dependent on L.

Specifically, there are three important parameters defined as follows:

- $X(r)$ represents the probability that a pore is occupied
- $X^A(r)$ represents the probability that a pore is part of a percolating cluster including the probability that a pore is part of a cluster that connects to the outer surface of the sample, but is not sample spanning.
- Coordination number Z is defined as the average number of neighboring pores to which a given pore is connected; in three dimensions, $Z = 1.5/p_c$ (Sahimi, 1993).

Each property can be determined using MICP output data. *X(r)* corresponds to the fraction of the pore system with capillary entry pressures less than or equal to the pore size *r* that is currently filled. $X^A(r)$ corresponds to the fraction of a pore system that is actually occupied at mercury pressures less than or equal to the capillary entry pressure of a pore size of *r*. These parameters can be found using the output of MICP test as follows.

$$X(r) = 1 - V(< r_{Hg}) \tag{1.29}$$

such that $X(r_{max}) = 0$ and where $V(< r_{Hg})$ is the cumulative probability density function and can be parameterized using Eqs. 2.2 and 2.6.

$$X^A(r) = \frac{\sum_{r_{min}}^{r} V_{pore,incremental}}{\sum_{r_{min}}^{r_{max}} V_{pore,incremental}} \tag{1.30}$$

using output volume taken from MICP measurements.

The relationship between *X(r)* and $X^A(r)$ is known as an accessibility function. In an infinite system, $X^A(r) = 0$ when $X(r) < p_t$ and approaches the slanted asymptote $X(r) = X^A(r)$ when $X(r) \gg p_t$. In finite systems, the accessibility function scales as a function of L and the asymptote is dependent on the value of the percolation threshold. Liu et al. (1992) present accessibility functions for cubic lattices of different sizes and coordination numbers and show that when *X* and X^A are multiplied by *Z*, the accessibility functions collapse onto a family of type curves. The shape of these functions depends solely on L and they are shown in Figure 2.2 along with the accessibility function for an infinite system.

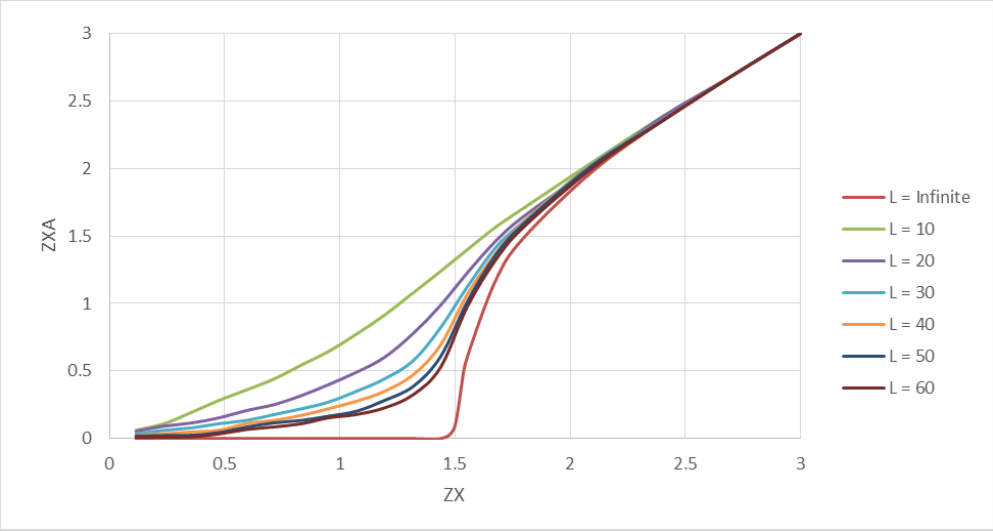

Figure 2.2: Accessibility functions presented in Liu et al. (Liu et al., 1992) showing variation in shape due to the effects of finite scaling.

Using these type curves and an iterative numerical solving tool built for this thesis, it is possible to optimize the value of L (and consequently p_c) and the variables used to parameterize the pore size distribution for any given unimodal system using MICP output data.

CHAPTER 3: METHODS AND DATA CORRECTIONS

3.1 MICP Results and Corrections

MICP data sets were taken for two separate samples of Berea Sandstone and one set of Racine Dolomite. The data was corrected for conformance effects in accordance with the procedure presented in Comisky et al. (2007) to ensure that pressure required to allow the mercury to surround or conform to the sample exterior without intruding into the pores did not interfere with results. Conformance effects were corrected using a plot of incremental pore volume occupied by mercury versus pore radius. Data points eliminated due to conformance effects shown alongside the pore volume distribution in Figure 3.1-3.3. A maximum radius r_{max} was then determined by calculating the point at which the linear trend beyond the peak in the unimodal distribution was projected to reach an incremental pore volume of zero.

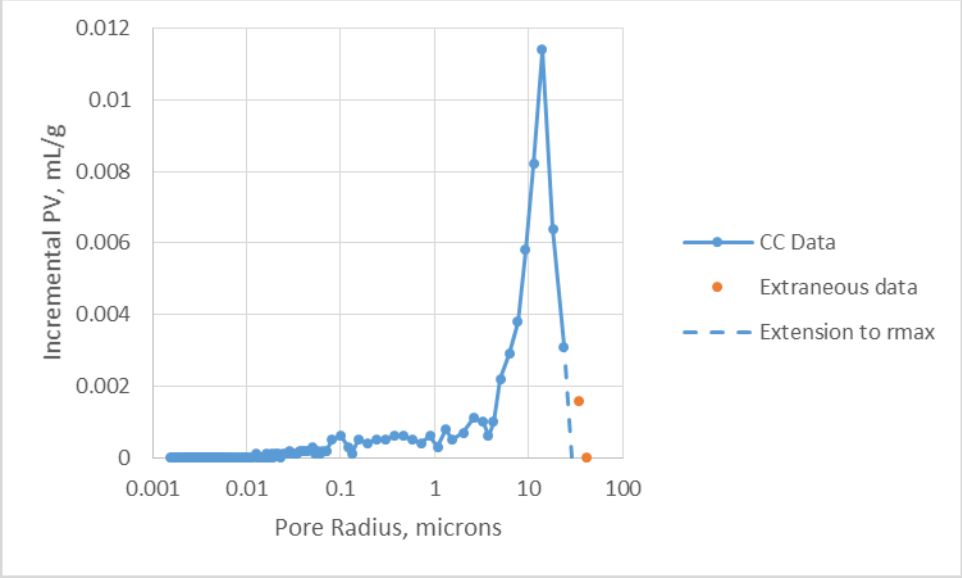

Figure 3.1: Incremental pore volume distribution of Berea_1 corrected for conformance effects. rmax located at (15.796, 0).

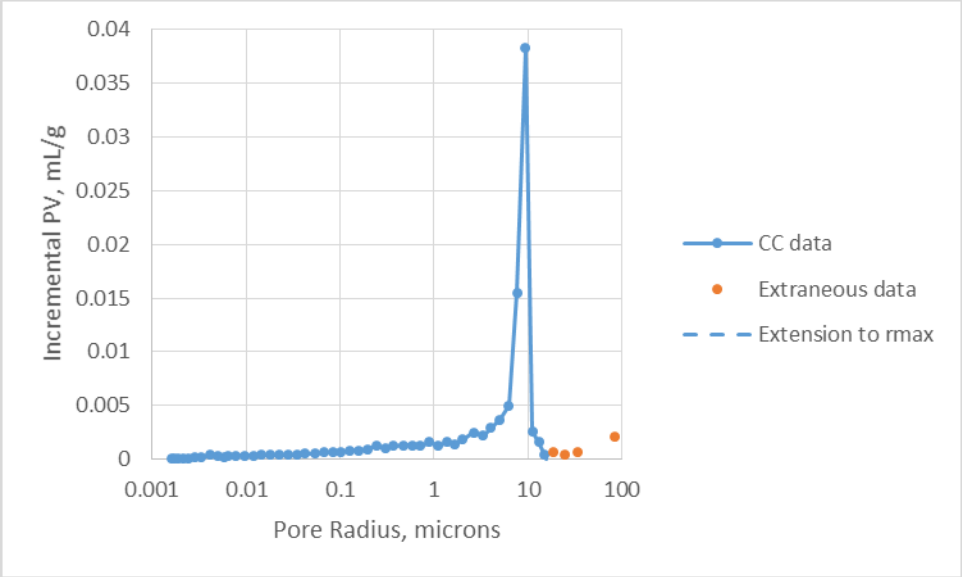

Figure 3.2: Incremental pore volume distribution of Berea_2 corrected for conformance effects. rmax located at (15.923, 0).

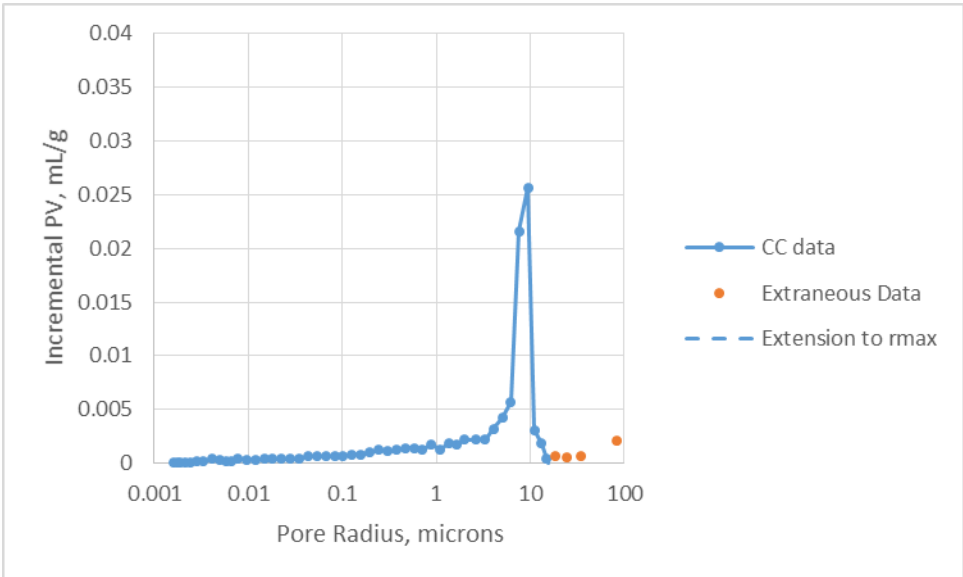

Figure 3.3: Incremental pore volume distribution of Racine Dolomite corrected for conformance effects. rmax located at (28.820, 0).

The uncorrected percolation threshold was identified as the point of maximum slope cumulative volume fraction of mercury intruded versus the capillary pressure for both sample sets (Katz & Thompson, 1987). These relationships are shown in Figures 3.4 - 3.6. Uncorrected percolation threshold data is shown in Tables 4.2 and 4.5.

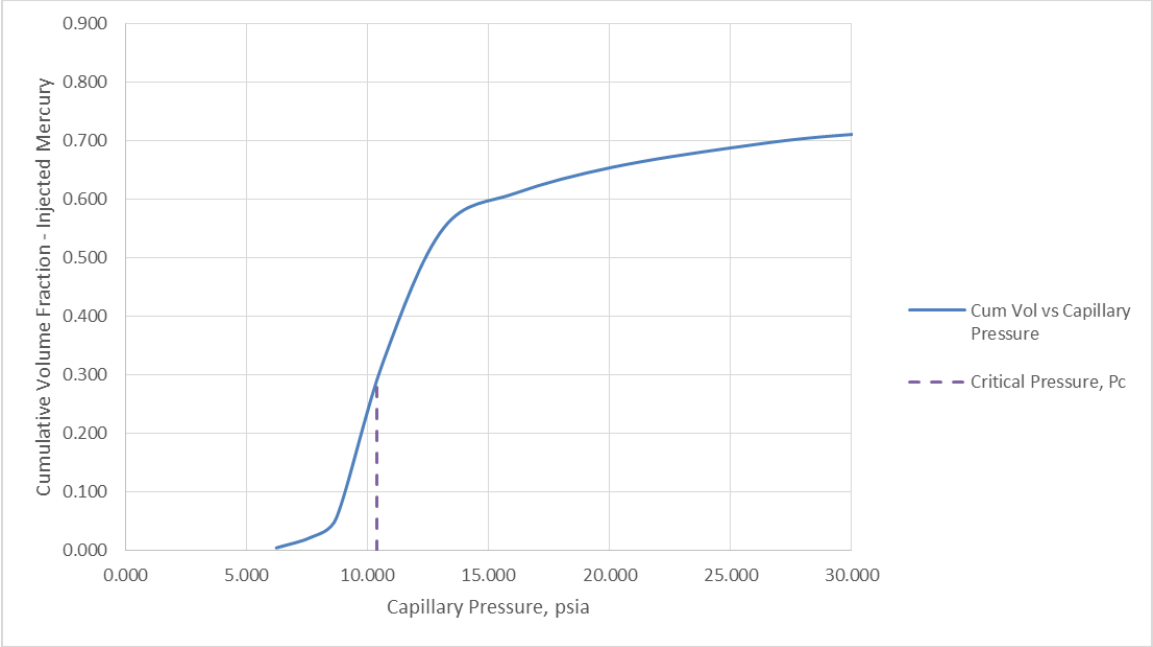

Figure 3.4: Cumulative Volume Fraction of Injected Mercury versus Capillary Pressure for Berea_1 Sandstone (Pc = 10.382 psia, pc(L) = 0.285)

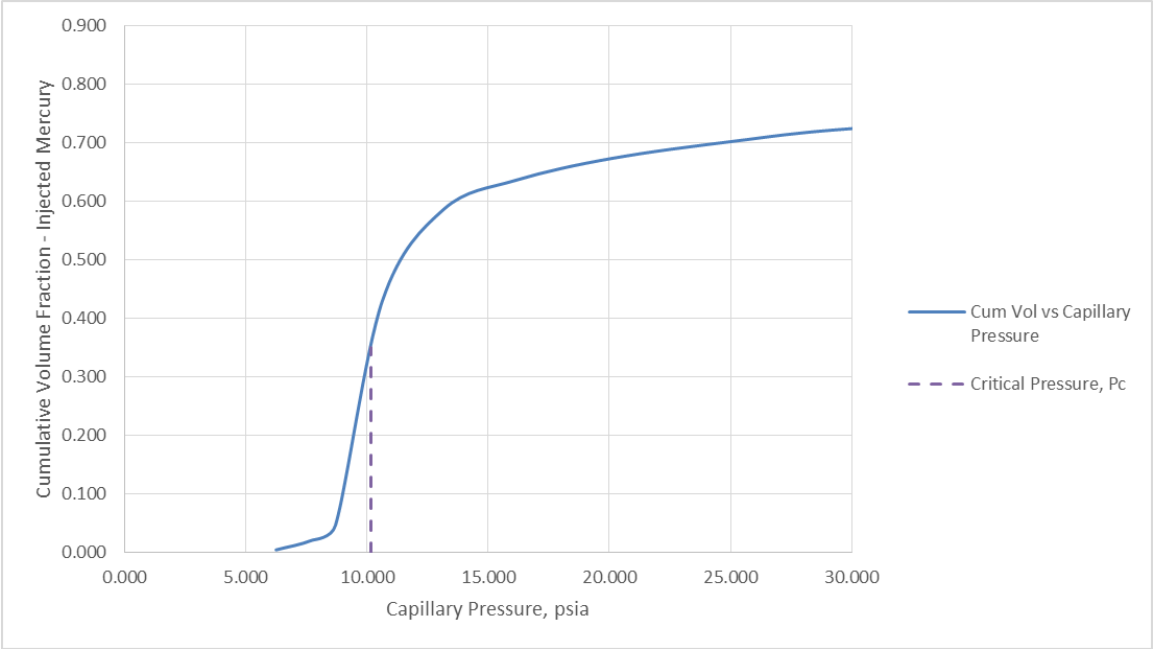

Figure 3.5: Cumulative Volume Fraction of Injected Mercury versus Capillary Pressure for Berea_2 Sandstone (Pc = 10.152 psia, pc(L) = 0.334)

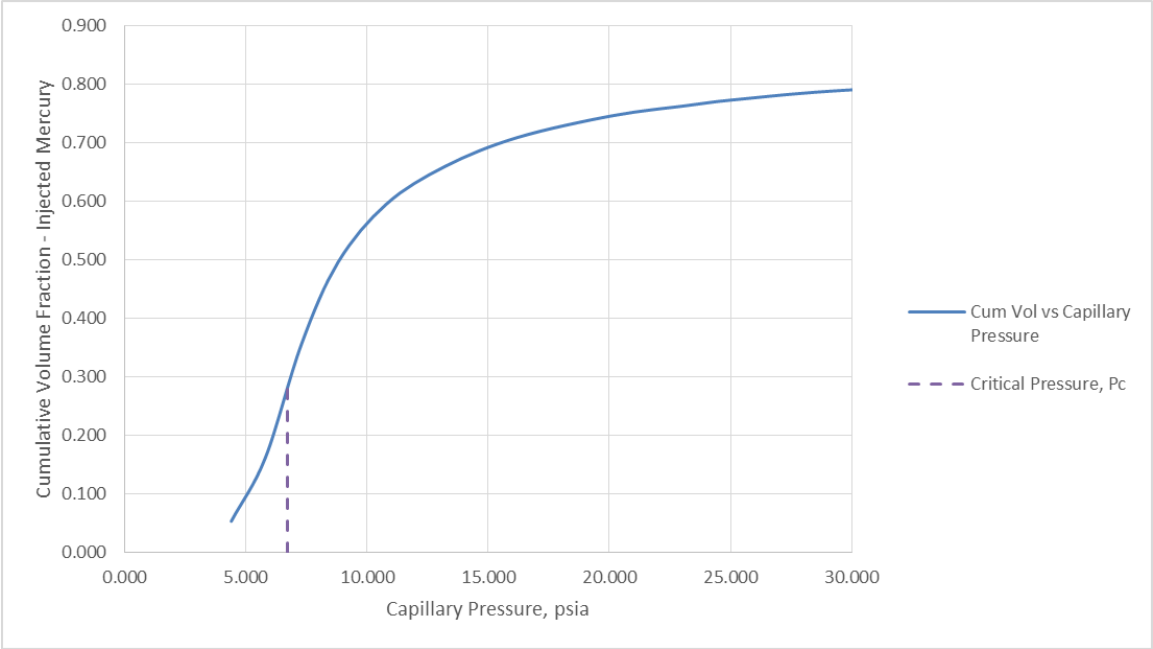

Figure 3.6: Cumulative Volume Fraction of Injected Mercury versus Capillary Pressure for Racine Dolomite (Pc = 6.703 psia, pc(L) = 0.278)

3.2 FORMATION FACTOR

Resistivity was determined using a Temco ECH-9 Resistivity Core Holder. Five sets of electric potential measurements were made using the core holder on Berea and Racine cores measuring ~0.5 cm in length and ~0.377 cm in diameter. Using the procedure presented in Section 2.5.1, formation factor values for each lithology were determined. Each core was dried, evacuated, and then saturated with a 3% NaCl brine solution. Resistivity of the saturating brine was measured as $R_w = 0.2386\,\Omega m$ using a Schlumberger Model EMT-2044 unit. The corresponding chart for this unit is shown in Figure A3.2 and operating instructions are included in Figure A3.3. The effective length between the two measurement locations was determined to be $L_{eff} = 0.0244$. Formation factor, potential measurements, and calculated resistivity results are summarized in Table A1.2. The calculated formation factors ($F_B = 15.821, F_R = 130.911$) were used in

determining parameters using known permeability values and can be considered as approximations for further prediction of permeability in Berea Sandstone and Racine Dolomite core samples. Once the corrected percolation threshold was determined for each set of parameters, the formation factor was used to calculate crossover porosity ϕ_x by rearranging Eq. 2.21. Crossover porosity values for each run can be found in Table A1.1.

3.3 Determining Parameters Using Known Permeability Values

3.3.1 Pore-Solid Fractal Model

Liu et al. (1992) used Monte Carlo simulations to show that the quantity $ZX^A(r)$ could be predicted from the quantity $ZX(r)$ by a scaling function whose form solely depends on L. Using this knowledge and known values of permeability, formation factor, and porosity, a method for determining pore-solid fractal method parameterization values β and D, along with other relevant parameterization values Z, c, and L works as follows.

The uncorrected percolation threshold $p_c(L)$ is determined from the MICP data. As described in previous sections, $X(r)$ was determined from MICP data as the cumulative fraction of the pore volume intruded with mercury starting from the low-pressure end of the data. A pore size r was assigned to each pressure point P by assuming cylindrical pores such that $r = (2\sigma|cos\theta|)/P$, with $\theta = 140°$ and $\sigma = 0.48$ N m^{-1} (Purcell, 1949). Thus, $X(r) = V(>r) = 1 - V(<r)$ where $V(<r)$ represented the volume fraction of pores that were smaller than r and was found using Eq. 2.2. Initial parametrization values were set according to Table A1.4. Then, $X^A(r)$, defined as the fraction of the pore system that is filled at any given pressure during an MICP test, was found using Eq. 2.29. Coordination number Z was set at an initial value of 3 and a plot of $ZX^A(r)$ versus $ZX(r)$ was created.

A knee value, or the point on the curve with the smallest distance to the percolation threshold for an infinite system ($ZX = 1.5$, $ZX^A = 0$), was defined for each accessibility function and the plot of $ZX^A(r)$ versus $ZX(r)$. These knee values were marked for each of the accessibility functions with x's as in Figure 3.7.

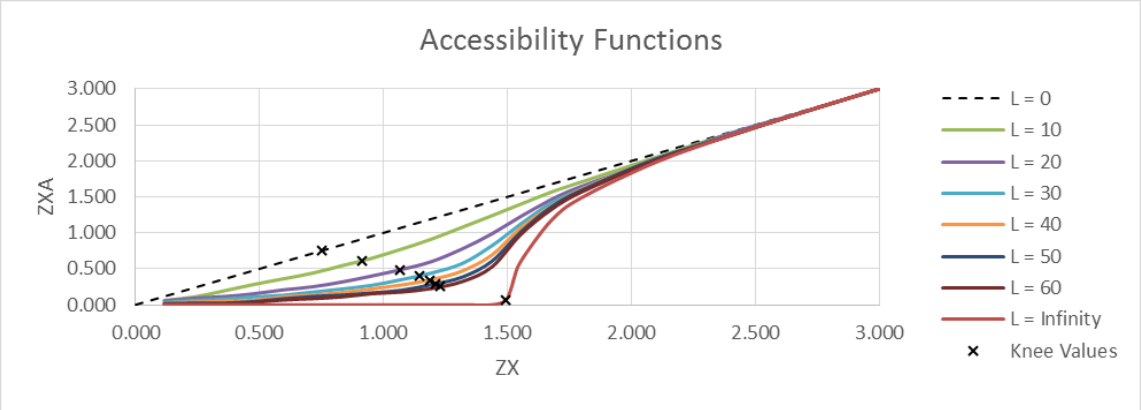

Figure 3.7: Accessibility functions with knee values shown

Coordinates for each knee value are plotted in Figure 3.8. When plotted, the knee values create an approximately linear trend described in Eq. 3.1 that matches the measured values with $R^2 = 0.9859$.

$$ZX^A = -0.9651ZX + 1.4868 \tag{1.31}$$

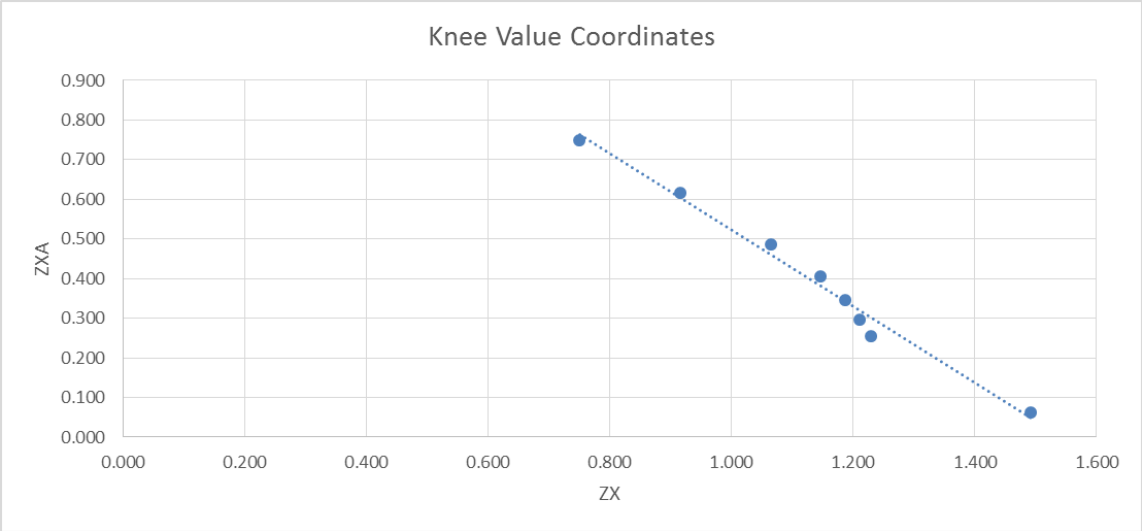

Figure 3.8: Linear trend of coordinates of the accessibility function knee values

Although values for parameterizing the pore size distribution (β, D) are available (Daigle, 2016a (Racine), 2016b (Berea)), they are dependent on the pore size distribution for the specific sample used in testing. In addition, it is widely accepted that for all three-dimensional lattices that Z can be approximated as $1.5/p_c$ where p_c is the percolation threshold (Sahimi, 1993). This, however, assumes that the percolation threshold is both known and corrected for finite scaling. I hypothesized that changing variables β, D, c and Z to simultaneously minimize the distance from the knee value to the trend shown in Eq. 3.1, collapse the shape of ZX^A versus ZX to the shape and range of the known accessibility functions, and match the calculated permeability with a known permeability for the sample would result in accurate parameters that could be used to calculate future permeability in the appropriate lithology.

The trend of the knee values is shown in Fig. 3.9 and was approximated with the following piece-wise power function

$$L = \begin{cases} 1.192 D_{pc}^{-0.314} & D_{pc} \leq 0.652 \\ 1.7195 D_{pc}^{-0.502} & D_{pc} > 0.652 \end{cases} \quad (1.32)$$

where D_{pc} is the distance from the infinite percolation threshold.

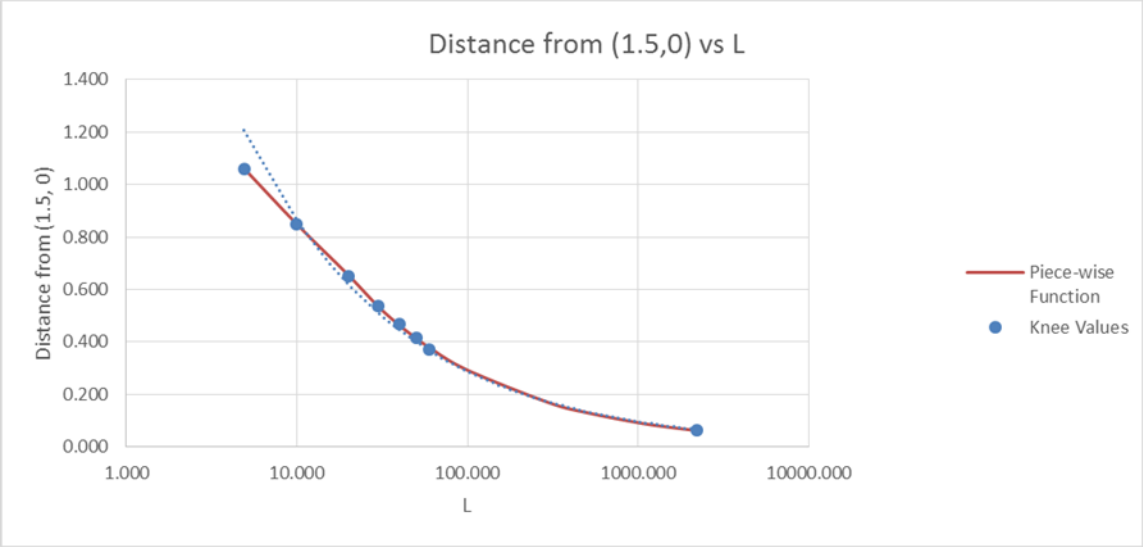

Figure 3.9: Power function of the distance from (1.5,0) of the knee values for the accessibility functions versus L. Prediction values are denoted with blue dashes and actual values are marked with green diamonds.

Corrected percolation threshold p_c was then determined using $p_c = aL^{-\frac{1}{\nu}} + p_c(L)$ where $a = 2.238$ and $\nu = 0.88$ (Daigle, 2016a). Finally, permeability k was found by substituting p_c, critical pore size r_c, and the optimized coefficient c into $k = (cr_c^2)/F$. As there are two separate ways of determining the critical pore size r_c (Eq. 2.4, Eq. 2.25), it was necessary to create two separate data sets. The two sets were created separately by substituting the corresponding r_c value into Eq. 2.27 and optimizing the resultant permeability to match a predetermined permeability value for the appropriate lithology.

For each set of MICP data and method of calculating critical pore size, β, D, c and Z were determined using multiple runs of Excel's evolutionary solver engine. The solver

constraints used for each sample are shown in Table A1.3. Results for these tests are detailed in Chapter 4.

The initial parametrization values came from Daigle (2016b) for Berea and Daigle (2016a) for Racine. These were determined by fitting Eq. 2.2 to a cumulative pore size distribution obtained from a combination of micro-CT images and NMR measurements. Porosity calculations for Berea and Racine ($\phi_B = 0.21, \phi_S = 0.197$) were determined by Boyle's law using helium. Permeability values ($k_B = 348\,md, k_S = 191.8\,md$) for comparison were determined by steady-state helium flow and corrected for gas slippage. Formation factor values were determined as described in Section 3.2 using a resistivity core holder. Uncorrected percolation threshold $p_c(L)$ values were determined from MICP data as described in Section 3.1. Combining β and D with r and r_{max} values taken from MICP data, an approximate pore size distribution was found using Eq. 2.1. In a similar fashion, $V(<r)$ was found by applying Eq. 2.2. Relevant plots of pore size distribution and $V(<r)$ versus r using calculated fitting parameters for Berea and Racine can be found in Figs. A2.1 – A2.5

3.3.1 Truncated Power Law Distribution

In investigations of CPA, authors have used several methods of parametrizing the pore-size distribution. While the pore-solid fractal model has been shown to be more appropriate for pore sizes in natural porous media, for the sake of comparison, I utilized same methodology that was applied in Section 3.3.1, but utilized a truncated power law distribution to formulate each of the relevant terms. The only differences between the two methods are defined as follows.

Rather than solve for parameterization values β and D, I used the distribution shape parameter α present in Eqs. 2.5 – 2.8 to constrain the data. Specifically, each of the terms

was calculated the same, however, different equations were used during parameterization. Thus, $X(r) = V(> r) = 1 - V(< r)$ where $V(<r)$ was found using Eq. 2.6. $X^A(r)$ was defined by the results of the MICP test and was still found using Eq. 2.29. Accessibility functions were independent of pore-size distribution, so the method for collapsing $ZX^A(r)$ versus $Zx(r)$ to the shape and range of the set of accessibility functions shown in Fig. 3.7 and calculating the corrected percolation threshold p_c using L was the same. Critical pore size was again defined in two ways, but this time it was defined by the Washburn Equation (Eq. 2.25) and using a truncated power law distribution (Eq. 2.8). Two sets of data were then created separately by substituting the corresponding r_c value into Eq. 2.27 and optimizing the resultant permeability to match a predetermined permeability value for the appropriate lithology.

Porosity calculations for Berea and Racine ($\phi_B = 0.21, \phi_S = 0.197$) were determined by Boyle's law using helium. Permeability values ($k_B = 348\, md, k_S = 191.8\, md$) for comparison were determined by steady-state helium flow and corrected for gas slippage. Formation factor values were determined as described in Section 3.2 using a resistivity core holder. Uncorrected percolation threshold $p_c(L)$ values were determined from MICP data as described in Section 3.1.

Initial parametrization values came from interpolated data to match pore-size distributions produced by Daigle (2016b) for Berea and Daigle (2016a) for Racine, obtained from a combination of micro-CT images and NMR measurements. These distributions were also used to determine r_{max} and r_{min} values. Fitting parameter α was used to fit Eq. 2.5 to the cumulative pore-size distributions and the result was taken as the guess value for each relevant data set.

CHAPTER 4: RESULTS AND ANALYSIS

4.1 DETERMINED PARAMETERS USING KNOWN PERMEABILITY VALUES

The following sections outline the results of the methods presented in Chapter 3, which attempt to utilize only MICP results and accessibility functions to determine a set of parameterization values that can be used to approximate permeability in the same lithology or a pore size distribution.

First, I present and analyze results of characterization using a pore-solid fractal model to parametrize the data for two Berea Sandstone samples and one Racine Dolomite sample. Next, I step through the same characterization using a truncated-power law distribution to parameterize the pore volume distribution of the same core samples.

Excel's evolutionary solver uses a genetic algorithm to apply thousands of continuously refined solutions within a set of defined constraints. It is not limited to complexity or linearity which makes it perfect for this application. The only shortcoming of the solver is that it provides a local solution when run, which may not represent a global solution and is highly dependent on the initial values provided. For this reason, it was necessary to run many iterations of the solver using the newly acquired parameters as initial parameters for the next run. In this way, optimal results were acquired.

4.1.1 Pore-Solid Fractal Model

Using the method defined in Section 3.3.1, the results summarized in Table 4.2 were produced. It bears noting that the $ZX^A(r)$ vs $ZX(r)$ curve was constrained using a point-by-point weighted average of the accessibility functions above and below the given data (denoted by L_{samp}). The closest accessibility functions were identified by matching the distance from the sample data knee value to the percolation threshold for an infinite system

($ZX = 1.5$, $ZX^A = 0$) to a distribution of the same distances for each of the accessibility functions.

For each sample, the solver was first run with permeability calculated using the Washburn equation to calculate r_c held constant (denoted as k_{wash}), then with permeability calculated using the PSF model to calculate r_c held constant (denoted as k_{psf}). This was completed for two samples of Berea (B_1 and B_2) and for one sample of Racine (R_1). Constraints set on Excel's solver during each run are shown in Table A4. Initial guess values for pore-solid fractal model parameters were taken from Daigle (2016b) for Berea and Daigle (2016a) for Racine. It is important to note that the geometrical constant c is known to vary based on the geometry of the pores and is found using the reduced constant parameters present in Eqs. 2.17 (cylindrical pores, base = 2, coefficient = 1/8) and 2.18 (slit-shaped pores base = 3, coefficient = 1/3). Skaggs (2011) noted that using an average value for these parameters produced feasible permeability solutions and eliminated the need for knowledge of the pore geometry. This average value ($c = 2.5^{-0.88}/5.5 = 0.081$) was the initial guess value supplied during optimization. All initial guess values are summarized in Table 4.1.

Sample	ϕ	β	D	c	Z	r_{min} (μm)	r_{max} (μm)
Berea_1	0.21	0.24	2.3	0.081	3.00	0.0022	15.80
Berea_2	0.21	0.24	2.3	0.081	3.00	0.0022	15.92
Racine	0.18	0.18	2.3	0.081	3.00	0.0050	28.82

Table 4.1: Initial solver entry values for solver using a pore solid fractal model for calculation of $V(<r)$. Berea – Daigle (2016b); Racine - Daigle(2016a)

Sample	$p_c(L)$	L	p_c	ϕ_x	β	D	c	Z	$r_{c,wash}$ (μm)	$r_{c,psf}$ (μm)	k_{wash} (m^2)	k_{psf} (m^2)
B_1,w	0.285	85.9	0.299	0.429	0.221	1.850	0.060	4.264	9.577	11.815	348.0	529.7
B_1,p	0.285	86.3	0.299	0.429	0.221	1.850	0.040	4.260	9.576	11.813	228.7	348.0
B_2,w	0.334	150.7	0.341	0.398	0.228	1.640	0.057	3.994	9.822	12.069	348.0	525.5
B_2,p	0.334	150.1	0.341	0.398	0.228	1.643	0.038	4.001	9.822	12.064	230.7	348.0
R_1,w	0.278	6.123	0.564	0.987	0.235	1.977	0.254	3.731	9.946	16.593	191.8	533.9
R_1,p	0.278	6.123	0.564	1.000	0.235	1.977	0.091	3.731	9.946	16.593	68.91	191.8
R_1,w,F	0.278	12.62	0.404	1.699	0.194	2.159	0.084	3.509	13.07	16.511	191.8	306.1
R_1,p,F	0.278	12.62	0.404	1.699	0.194	2.159	0.053	3.509	13.07	16.511	120.2	191.8

Table 4.2: Resultant parameters solving for known permeability ($k_B = 348.0\ md$,$k_R = 191.8\ md$) with initial values as defined in Table 3 and solver constraints as defined in Table A4. Subscripts w and p stand for the two methods for calculating critical pore size (Washburn Equation (Eq. 2.23) and Pore Solid Fractal derivation (Eq. 2.4) respectively)

Appropriate results can visualized by overlaying the trend of $ZX^A(r)$ vs $ZX(r)$ for the sample onto the accessibility functions. A good match is seen as a match in shape and range along these curves. Examples of these distributions are shown in Fig. 4.1, 4.2, and 4.3 for Berea_1, Berea_2, and Racine respectively.

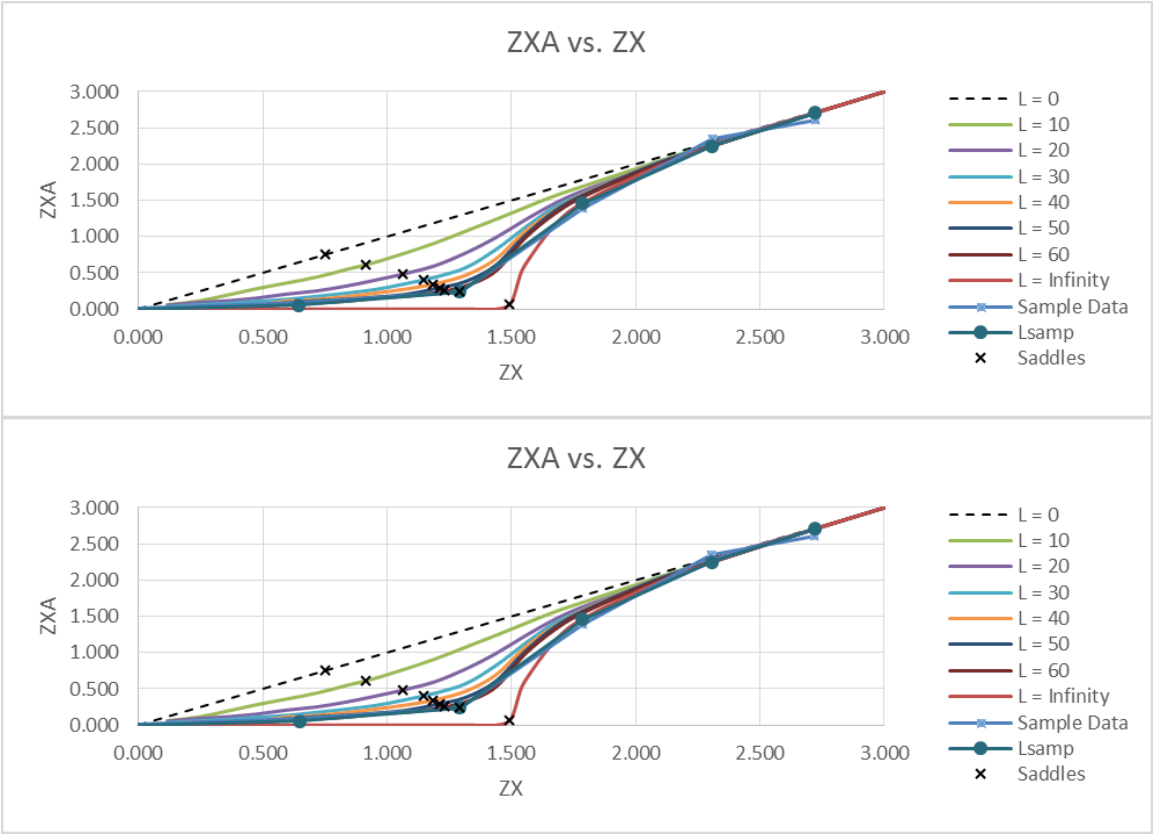

Figure 4.1: (Top) ZXA(r) vs ZX(r) for Berea_1 sample with solver permeability calculated using Washburn's equation (Eq. 2.23); (Bottom) ZXA(r) vs ZX(r) for Berea_1 sample with solver permeability calculated using the pore solid fractal model (Eq. 2.8)

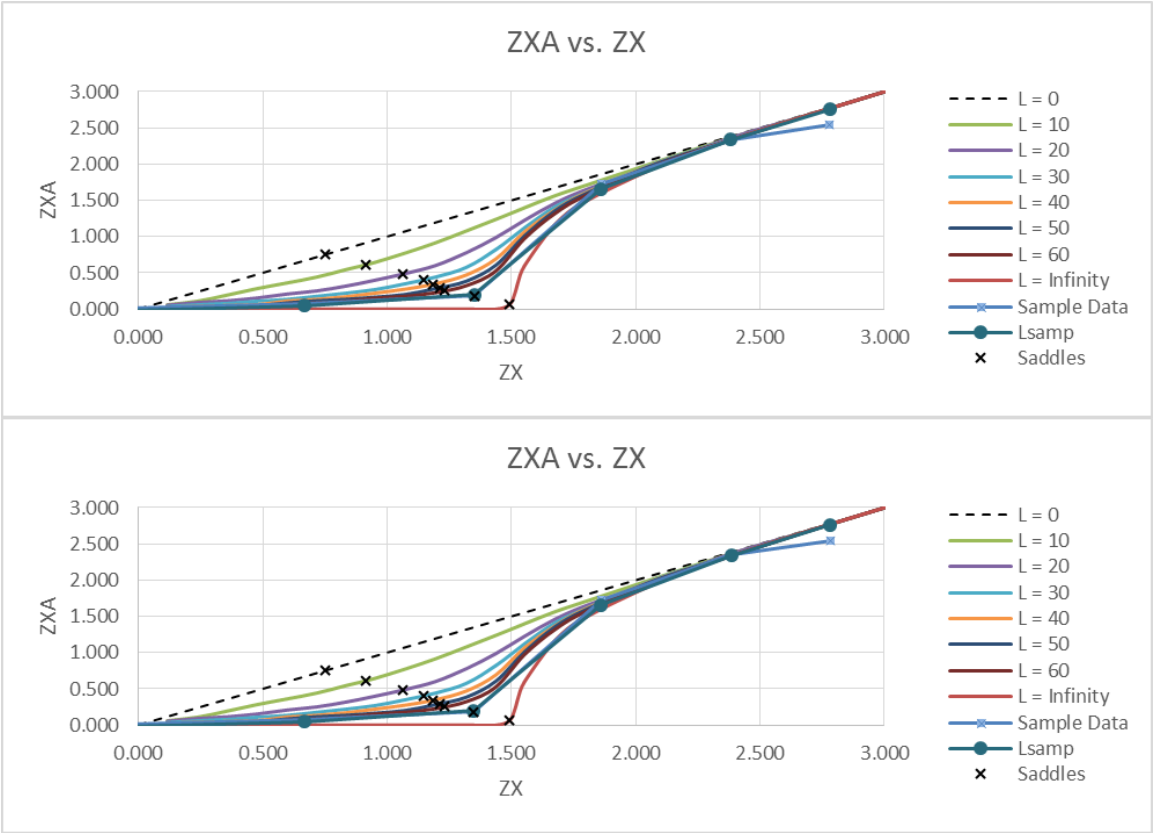

Figure 4.2: (Top) ZXA(r) vs ZX(r) for Berea_2 sample with solver permeability calculated using Washburn's equation (Eq. 2.23); (Bottom) ZXA(r) vs ZX(r) for Berea_2 sample with solver permeability calculated using the pore solid fractal model (Eq. 2.4)

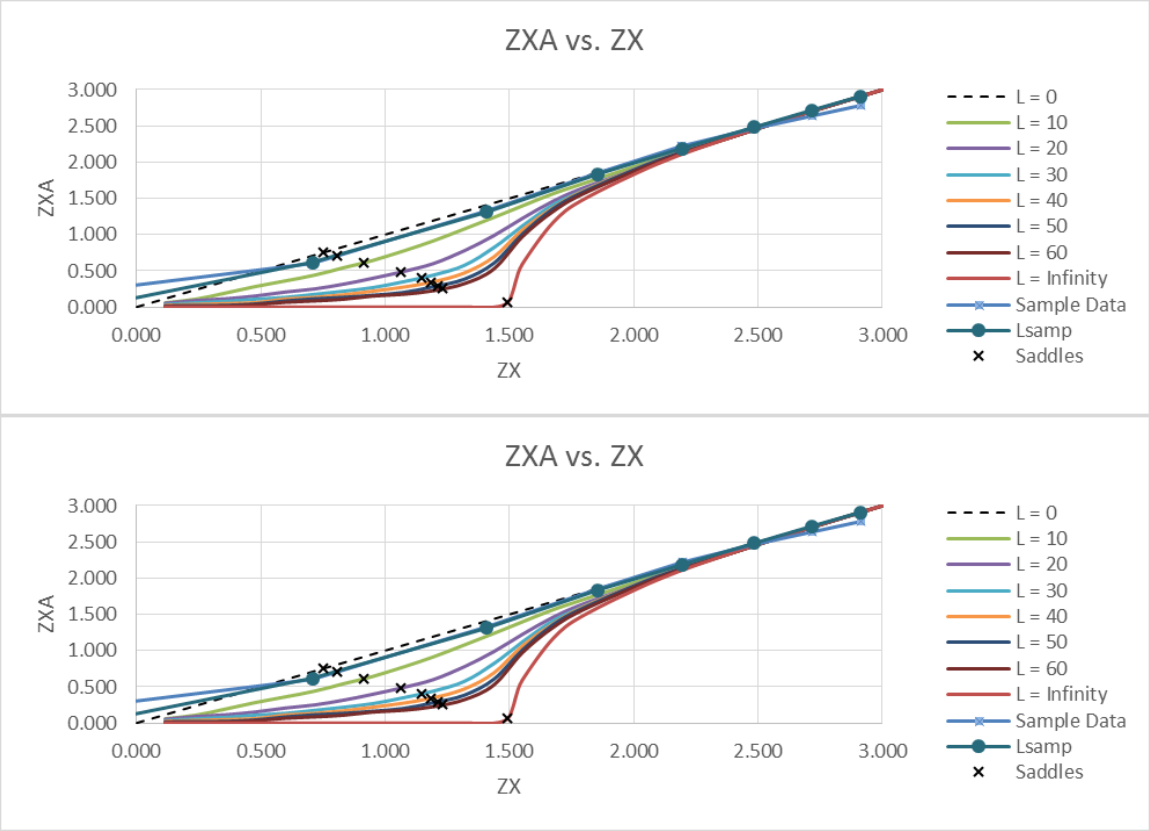

Figure 4.3: (Top) ZXA(r) vs ZX(r) for Racine sample with solver permeability calculated using Washburn's equation (Eq. 2.23); (Bottom) ZXA(r) vs ZX(r) for Racine sample with solver permeability calculated using the pore solid fractal model (Eq. 2.4)

Visually, it is obvious that not only do the resultant $ZX^A(r)$ vs ZX(r) curves for Berea_1 and Berea_2 shown in Figures 4.1 and 4.2 collapse well onto the accessibility function type curves, they also match each other. Numerically, however, examining permeability results yields different results based on the method used for determining critical pore size. Specifically, k_{psf} is greater than k_{wash} by a factor of 1.52 in Berea_1, 1.51 in Berea_2, and 2.78 in Racine. This difference is accounted for by the variance in c values by the same factor for each sample. Since constant c is known to vary with pore geometry, I determined that comparing the necessary base and denominator to produce the resultant

c values may indicate which method of calculating critical pore size was more appropriate. Comparisons of denominators were made using the equation $denom = 2.5^{-0.88}/c$, which comes from the definition of constant *c* in Section 2.5.3, assuming a base of 2.5. Based on the findings of Skaggs (2011), denominators should fall between 3 and 8. Values for each run are summarized in Table 4.3.

Sample	*c*	*base*	*denom*	c_i/c_{wash}
Berea_1,w	0.060	2.5	7.437	1.000
Berea_1,p	0.040	2.5	11.316	1.522
Berea_2,w	0.057	2.5	7.824	1.000
Berea_2,p	0.038	2.5	11.802	1.509
Racine,w	0.259	2.5	1.759	1.000
Racine,p	0.117	2.5	4.896	2.780
Racine,w,F	0.084	2.5	5.326	1.000
Racine,p,F	0.053	2.5	8.500	1.596

Table 4.3: Calculated denominator necessary for the set constant c values to match the equation $c = 2.5^{-0.88}/denom$. Note that base values are set at an average of base values for cylindrical (base = 2) and slit-shaped pores (base = 3) and calculations were made with a crossover porosity set at a maximum of 1 (Skaggs, 2011). Subscripts w and p stand for the two methods for calculating critical pore size (Washburn Equation (Eq. 2.23) and Pore Solid Fractal derivation (Eq. 2.4) respectively)

The data in Table 4.3 suggests that in Berea samples, using the Washburn equation yield results that fall within the range of pore geometry recommended by Skaggs (2011). This suggests that the solution given by the Washburn equation may be more feasible in calculating permeability

It is puzzling to note that in the Racine sample the Washburn geometrical denominator did not fall between the expected range of 3 to 8 and that the factor c_i/c_{wash} was significantly different from the other samples analyzed. I analyzed the solver constraints in order to identify a potential source of this discrepancy.

One important constraint used when determining in the optimized parameters shown in Table 3 was the supposition that $\phi_x \leq 1$, determined by rearranging Eq. 2.21 to solve for crossover porosity. Physically, this is logical as the crossover porosity represents the porosity at which the scaling of electrical conductivity crosses from percolation theory to effective medium theory and porosity cannot represent a value greater than 1. However, formation factor was determined using a resistivity core holder for all samples, so the constraint was unnecessary to use. In Berea samples, this constraint did not affect results because the crossover porosity was well below a value of 1, whereas removing this constraint in Racine samples resulted in a significantly better match when comparing the plot of $ZX^A(r)$ versus ZX(r) with accessibility functions.

Assuming that Eq. 2.21 is accurate and valid for all samples used in this thesis, ϕ_x can be determined using the recalculated parameters (F, ϕ, and p_c). As was previously mentioned, a crossover porosity greater than 1 does not make physical sense implying that one of the other constraints may be inaccurate. Formation factor is the only physical parameter determined from a separate set of core samples making it the most likely to be incorrect. With this in mind, I recalculated Eq. 2.21 with $\phi_x = 1$, $\phi = 0.18$, and $p_c = 0.404$, and found that $F = 74.66$. To account for this change, constant c was updated and results denoted with an "F" in Tables 4.2 and 4.3 were produced. For these updated parameters, the $ZX^A(r)$ vs ZX(r) curve matches the shape of the accessibility functions very well as shown in Figure 4.4 and the geometrical coefficient denominator is well within the feasible range of 3 to 8 for both variations of calculating critical pore size.

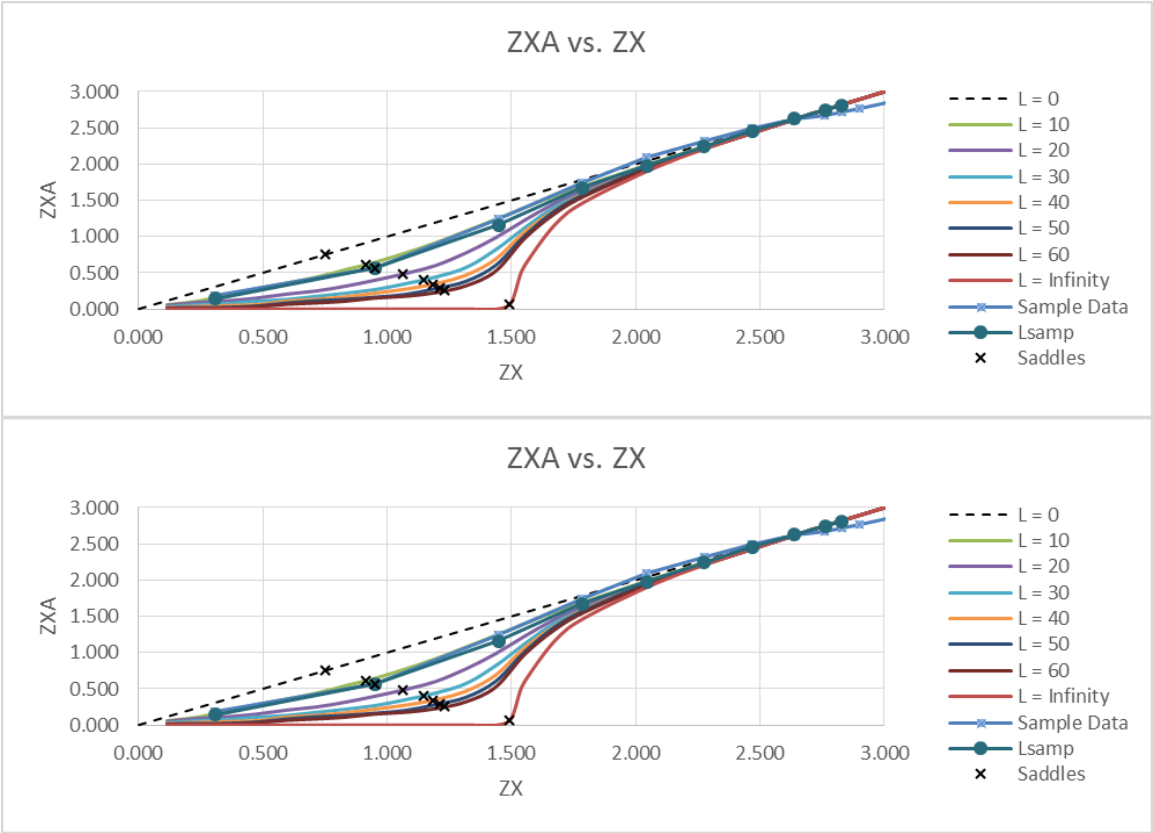

Figure 4.4: (Top) Updated ZXA(r) vs ZX(r) for Racine sample with solver permeability calculated using Washburn's equation (Eq. 2.23); (Bottom) ZXA(r) vs ZX(r) for Racine sample with solver permeability calculated using the pore solid fractal model (Eq. 2.12). Solver constraint of $\phi_x \leq 1$ was omitted.

4.1.2 Truncated Power Law Distribution

Using the same methods applied in 4.1.1 with PSF model equations Eqs. 2.1 - 2.4 updated to match Eqs. 2.5 – 2.8 developed from a truncated power law distribution, results were shown in Table 4.5 were found. Initial solver entries were set using the values shown in Table 4.4.

Sample	ϕ	α	c	Z	r_{min} (μm)	r_{max} (μm)
Berea_1	0.21	-0.6	0.081	3.000	0.0022	15.80
Berea_2	0.21	-0.6	0.081	3.000	0.0050	15.92
Racine	0.18	-0.6	0.081	3.000	0.0050	28.82

Table 4.4: Initial solver entry values for solver using a truncated power law distribution for calculation of *V(<r)*. Berea – Daigle (2016b); Racine - Daigle(2016a).

Sample	$p_c(L)$	L	p_c	ϕ_x	α	c	Z	$r_{c,wash}$ (μm)	$r_{c,tpl}$ (μm)	k_{wash} (m^2)	k_{tpl} (m^2)
B_1,w	0.285	93.05	0.298	0.043	-0.055	0.060	4.139	9.584	11.30	348.0	483.6
B_1,p	0.285	93.05	0.298	0.043	-1.055	0.043	4.139	9.584	11.30	250.4	348.0
B_2,w	0.334	168.2	0.340	0.399	-1.209	0.057	3.818	9.826	11.29	348.0	459.3
B_2,p	0.334	168.2	0.340	0.399	-1.209	0.043	3.818	9.826	11.29	263.2	348.0
R_1,w	0.277	6.096	0.564	1.000	-0.437	0.257	3.942	9.889	4.518	191.8	40.04
R_1,p	0.277	6.096	0.564	1.000	-0.437	1.230	3.942	9.889	4.518	918.8	191.8
R_1,w,F	0.277	17.32	0.364	1.000	-0.791	0.067	3.330	13.78	16.25	191.8	266.7
R_1,p,F	0.277	17.32	0.364	1.000	-0.791	0.048	3.330	13.78	16.25	137.9	191.8

Table 4.5: Resultant parameters solving for known permeability ($k_B = 348.0\ md$,$k_R = 191.8\ md$) with initial values as defined in Table A2 and solver constraints as defined in Table A4. Subscripts w and p stand for the two methods for calculating critical pore size (Washburn Equation (Eq. 2.23) and Pore Solid Fractal derivation (Eq. 2.4) respectively)

Percolation threshold p_c values and length the media L match well with those determined using a PSF model. Again, matching data can be visually recognized by observing how well the plot of $ZX^A(r)$ vs $ZX(r)$, calculated using resultant parameters, collapsed onto the accessibility functions. Examples of this are shown in Fig. 4.5, 4.6, and 4.7 for Berea_1, Berea_2, and Racine respectively. Comparisons of the constant c and necessary denominator with a base set to 2.5 are shown in Table 4.8.

Sample	c	*base*	*denom*	c_i/c_{wash}
Berea_1,w	0.060	2.5	7.448	1.000
Berea_1,p	0.043	2.5	10.352	1.390
Berea_2,w	0.057	2.5	7.829	1.000
Berea_2,p	0.043	2.5	10.352	1.320
Racine,w	0.257	2.5	1.738	1.000
Racine,p	1.230	2.5	0.363	0.209
Racine,w,F	0.067	2.5	6.630	1.000
Racine,p,F	0.048	2.5	9.219	1.390

Table 4.8: Calculated denominator necessary for the set constant c values to match the equation $c = 2.5^{-0.88}/denom$. Note that base values are set at an average of base values for cylindrical (base = 2) and slit-shaped pores (base = 3) and calculations were made with a crossover porosity set at a maximum of 1 (Skaggs, 2011). Subscripts w and p stand for the two methods for calculating critical pore size (Washburn Equation (Eq. 2.23) and Pore Solid Fractal derivation (Eq. 2.4) respectively)

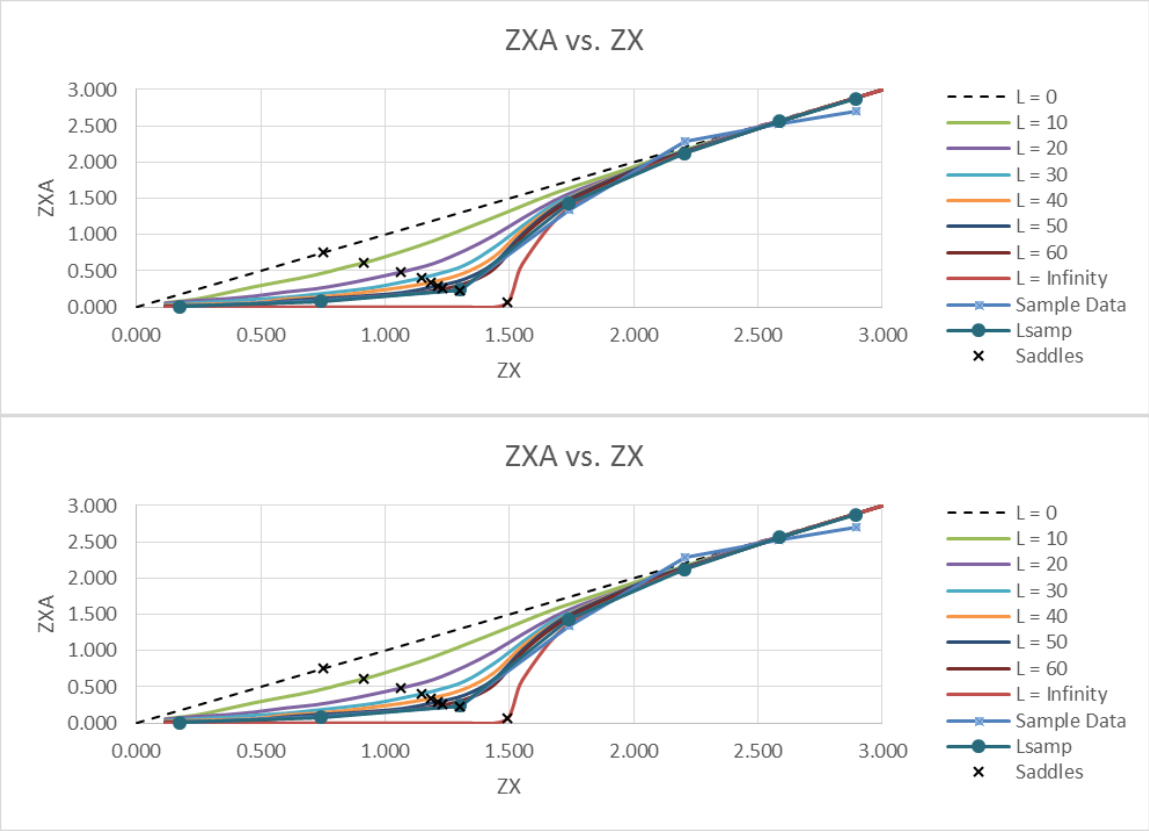

Figure 4.5: (Top) ZXA(r) vs ZX(r) for Berea_1 sample with solver permeability calculated using Washburn's equation (Eq. 2.23); (Bottom) ZXA(r) vs ZX(r) for Berea_1 sample with solver permeability calculated using a truncated power law distribution (Eq. 2.8)

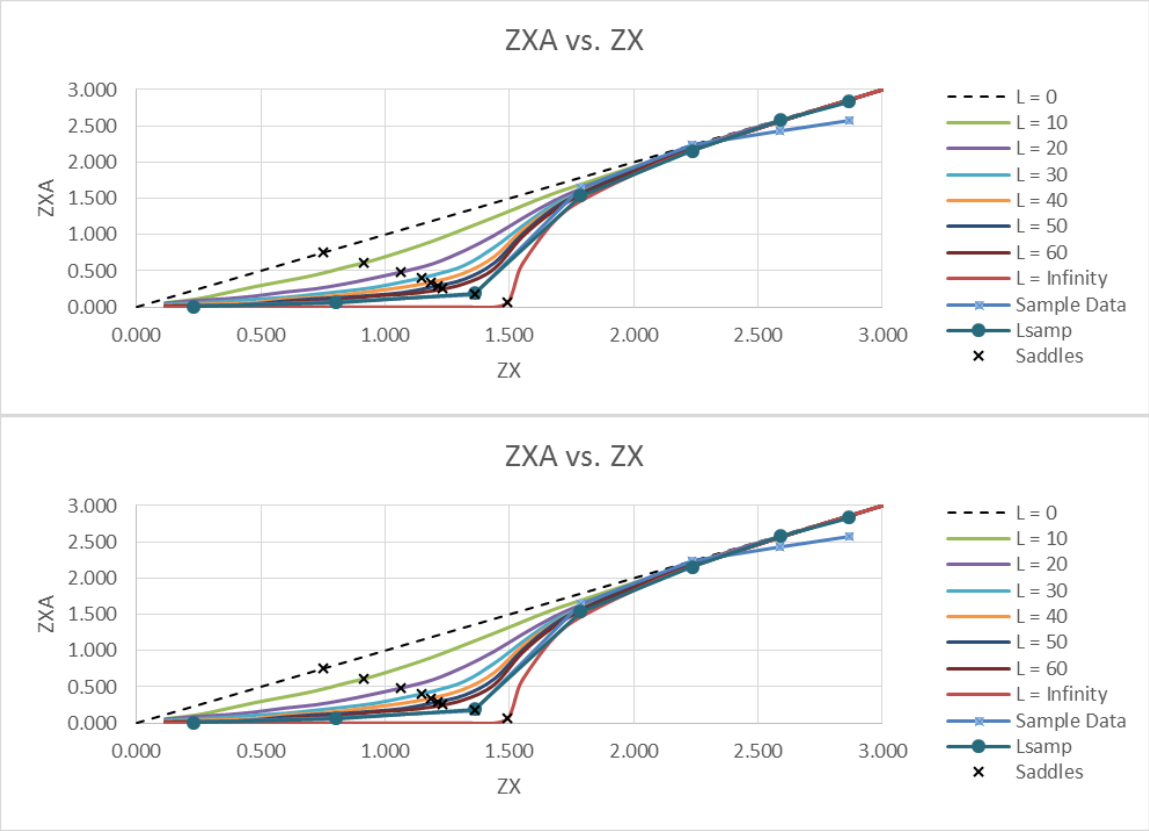

Figure 4.6: (Top) ZXA(r) vs ZX(r) for Berea_2 sample with solver permeability calculated using Washburn's equation (Eq. 2.23); (Bottom) ZXA(r) vs ZX(r) for Berea_2 sample with solver permeability calculated using a truncated power law distribution (Eq. 2.8)

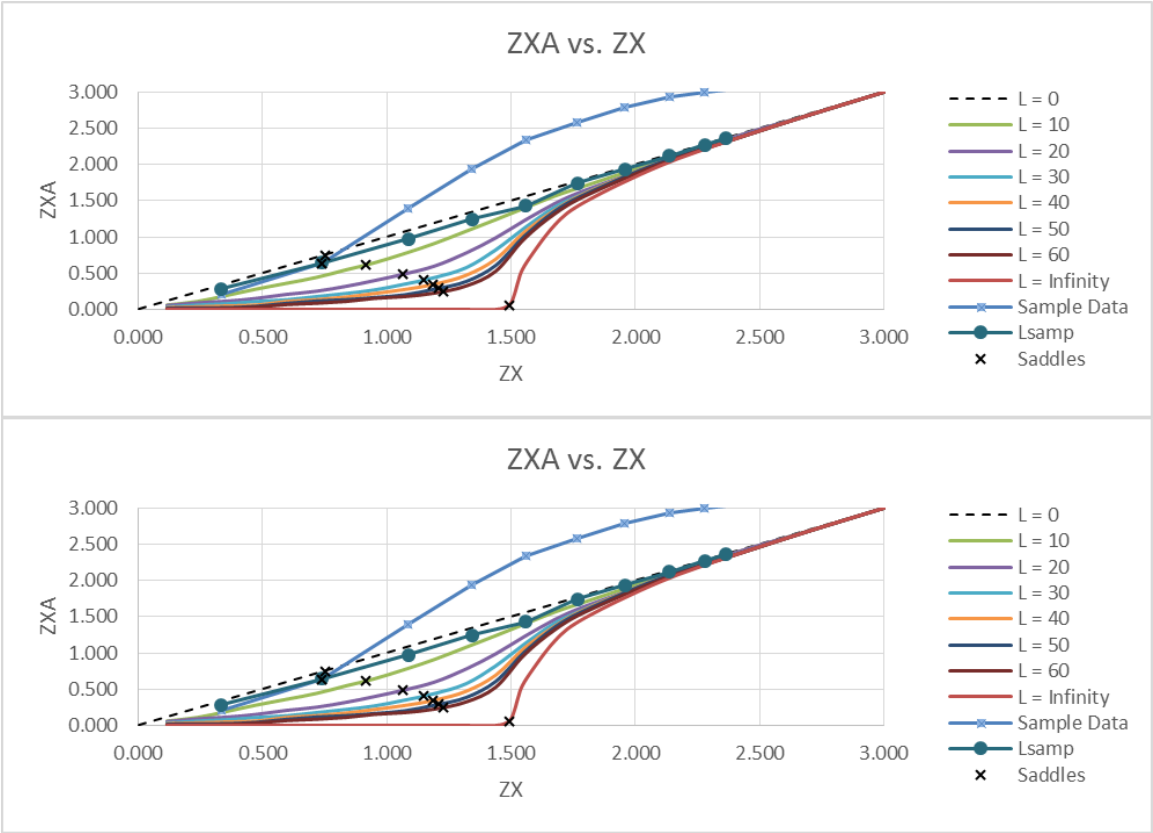

Figure 4.7: (Top) ZXA(r) vs ZX(r) for Racine sample with solver permeability calculated using Washburn's equation (Eq. 2.23); (Bottom) ZXA(r) vs ZX(r) for Racine sample with solver permeability calculated using a truncated power law distribution (Eq. 2.8)

The issues with Racine discussed in the previous section are amplified using a TPL distribution to parametrize the data because there is only one variable, distribution shape parameter α used to constrain the shape of the curve as shown in Figure 4.7. Running the solver again with the constraint $\phi_x \leq 1$ removed, then recalculating formation factor F using the results and with ϕ_x set to 1, values denoted with "F" in Tables 4.4 and 4.5 were produced. Recalculated formation factor was determined to equal 66.7. The $ZX^A(r)$ vs ZX(r) for this recalculation is shown in Figure 4.8.

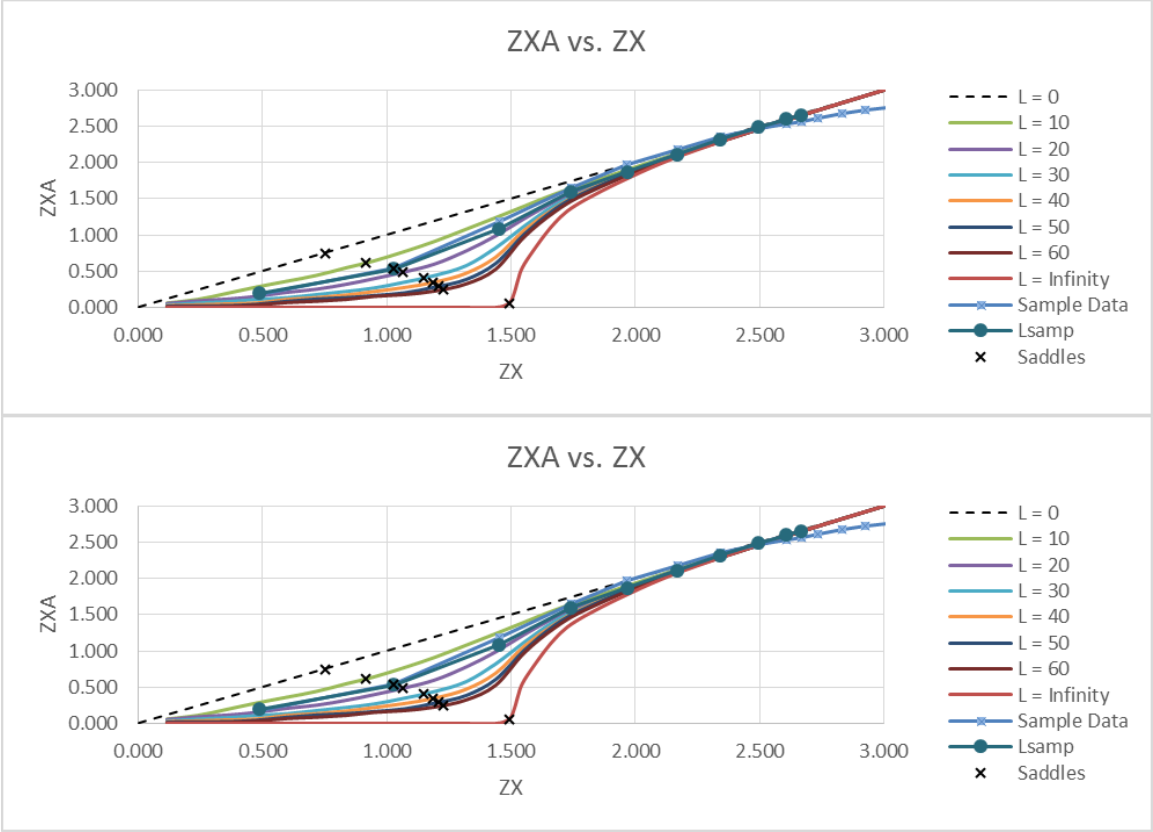

Figure 4.8: (Top) Updated ZXA(r) vs ZX(r) for Racine sample with solver permeability calculated using Washburn's equation (Eq. 2.23); (Bottom) ZXA(r) vs ZX(r) for Racine sample with solver permeability calculated using a truncated power law distribution (Eq. 2.8). Solver constraint of $\phi_x \leq 1$ was omitted.

Further support for the recalculated data without the $\phi_x \leq 1$ constraint in place can be found by observing plots of the cumulative probability density functions and volumetric probability density plots created using corresponding PSF models and TPL distributions. These can also be compared to distributions created from parameterization values taken from the literature. In theory, PSF and TPL models should display similar distributions, however, Figure 4.9 and 4.10 show that with the $\phi_x \leq 1$ constraint in place there are large discrepancies between the two model distributions. Removing the constraint and

recalculating the formation factor with crossover porosity set to 1 brings the distributions together almost perfectly in the cumulative probability density functions shown in Fig. 4.9 and much closer in the pore size distributions shown in Fig. 4.10.

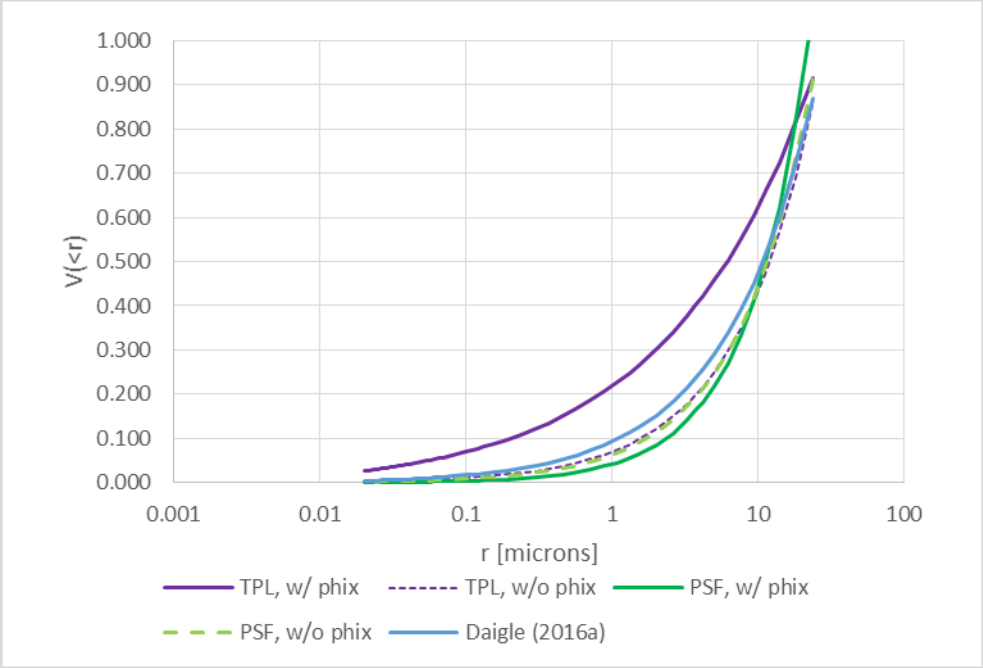

Figure 4.9: Comparison of cumulative probability distribution calculated using a PSF model and TPL distribution with and without the constraint $\phi_x \leq 1$ present.

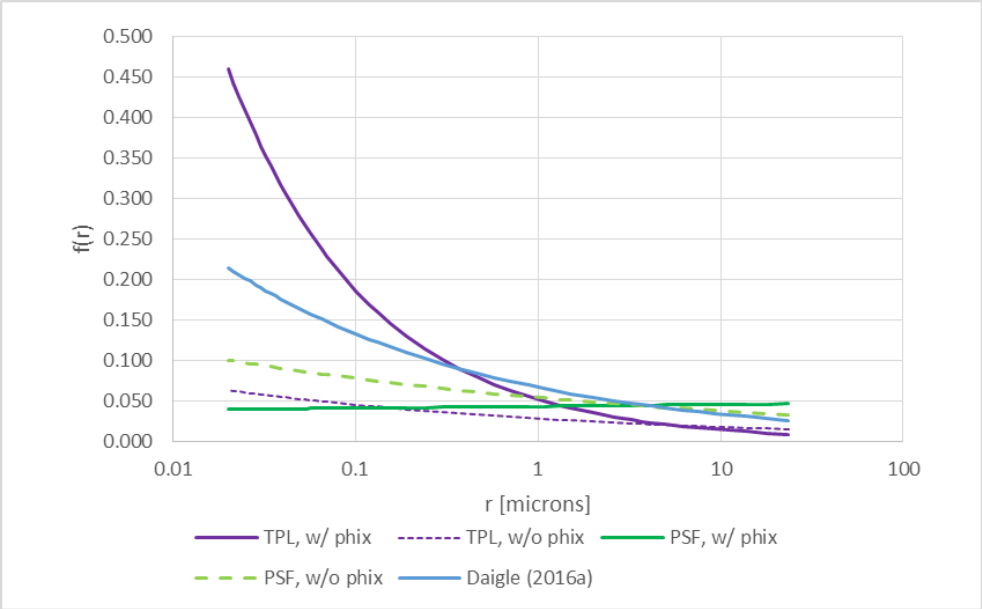

Figure 4.10: Comparison of volumetric probability density calculated using a PSF model and TPL distribution with and without the constraint $\phi_x \leq 1$ present.

A literature distribution for Racine was created using parameterization values and r_{max} taken from Daigle (2016a) and compared to the distributions created in this thesis. A clear match is observed and slight variations are only present due to the slight difference in maximum pore size between sample and literature values (~28 µm versus ~30 µm).

A literature distribution for Berea was created using parameterization values taken from Daigle (2016b) and an r_{max} value taken from Daigle (2016a), however the substantial difference between sample and literature r_{max} values made it difficult to compare. Instead, an r_{max} value equal to that in the literature (30 µm) was assumed and the methods presented in this thesis were used to approximate V(<r) and f(r), which were compared to the distributions defined by the literature values. The $ZX^A(r)$ vs ZX(r) for sample and literature data for Berea_1 and Berea_2 samples are presented in Appendix Figures B5 and B8 respectively. Cumulative probability distribution and volumetric probability density comparisons for Berea_1 and Berea_2 are also present in Appendix B.

4.2 Comments on Critical Pore Size Calculation Methods

Tables 4.3 and 4.8 show comparisons of the constant *c* and necessary denominator for the definition of *c* presented in Section 2.5.3 with a base set to 2.5. These are directly correlated to the ratio of k_{psf}/k_{wash} and therefore also directly proportional to the ratio of r_{psf}/r_{wash}. Disregarding calculations made with the constraint $\phi_x \leq 1$ in place for Racine, a ratio of ~1.55 and ~1.35 was displayed across all samples for PSF model and TPL distribution respectively. This suggests that there may be a correction factor necessary when applying a distribution to solve for critical pore size. The difference may also be due to the assumption of cylindrical pores made when applying the Washburn equation. Regardless, more work will need to be completed to analyze this difference fully.

CHAPTER 5: CONCLUSIONS AND RECOMMENDATIONS

The methods presented in this thesis are only applicable to highly heterogeneous, sufficiently diverse, and unimodal distributions. Methods were applied to test results for core samples taken from Berea sandstone and Racine dolomite lithologies.

5.1 CONCLUSIONS

The overall goal of this thesis was to provide further insight into the calculation of permeability in porous media using Critical Path Analysis. This was accomplished by first recognizing critical pore size and the length of the medium to be two fundamental length scales in determining permeability and then using this knowledge to constrain parametrized MICP data to the form of accessibility functions. These characteristic curves, when combined with coordination number Z, define the relationship between the probability that a pore is occupied and the probability that the same pore is part of a percolating cluster.

I hypothesized that since the shape and scale of accessibility functions have been shown to solely depend on length of porous medium L and percolation threshold p_c, parameterizing these two variables using a pore solid fractal model or truncated power law distribution and constraining parameterization values to match accessibility functions should result in reasonable, lithology specific variables that can be applied in the future to approximate permeability or a pore size distribution. Both the permeability calculation and correction for finite scaling can be carried out without an independent pore size distribution measurement.

Results of these methods were obtained for both a PSF model and TPL distribution and resulting parameterization values were used to create cumulative probability distribution functions. These were then compared to distributions created from parameters

taken from literature. For Racine samples, these distributions matched well. Substantial differences were present in the Berea samples because significant differences in maximum pore size were present between my data and the literature values.

It was also shown that when critical pore size was quantified using PSF model or TPL distribution parameterization values, the result was consistently larger than calculations made using the Washburn equation by a constant factor across all samples tested. The constant varied slightly between parametrization methods. This observation suggests that it is possible to only use parametrization values to approximate critical pore size, although a correction factor may be necessary.

Overall, the work completed for this thesis confirms that Critical Path Analysis can be a viable method in determining permeability for highly heterogeneous porous media. In doing so, relevant parameters affecting permeability are reduced to Formation factor, critical pore size, and a constant dependent on pore geometry. Using methods presented in this thesis, all that would be necessary for accurately approximating permeability in a given sample would be mercury intrusion capillary pressure (MICP) data, knowledge of the formation factor for the specific lithology, and a set of predetermined parameters, provided that porosity is known and the lithology displays a unimodal pore size distribution. This is significant because it alleviates the need to have a measured pore size distribution which could help reduce the time and number of tests necessary to determine permeability.

5.2 Ideas For Future Work

There are a number of ways to expand on the research presented in this thesis. First, more MICP tests need to be taken on both Berea sandstone and Racine Dolomite lithologies in order to confirm shape parameters determined using a PSF model and TPL distribution in order to create parameters that can confidently be used in concert with new data sets to

predict permeability. The idea that MICP data can be constrained to fit the shape of accessibility functions and used to output volumetric density distributions is relatively new and can only be solidified by examining more data. It would also be beneficial to use these data sets to examine the difference between calculating critical pore size using the Washburn equation or using the corresponding distribution to derive an equation for critical pore size as I began to do in Section 4.2. Finally, the methods for determining shape parameters to predict permeability can be applied to other lithologies as long as they are highly heterogeneous and exhibit a wide, but unimodal pore size distribution. Methods for dealing with lithologies exhibiting bimodal or other types of pore size distribution were not covered in this thesis and need to be studied further in order to apply the ideas presented here.

APPENDIX A

	Berea	Racine
diam [m]	0.038	0.038
L [m]	0.051	0.049
V_1 [V]	5.370	5.070
	10.190	10.040
	15.270	15.050
	20.140	20.040
	25.030	25.070
V_2 [V]	0.444	3.580
	0.840	6.980
	1.263	10.310
	1.662	13.560
	2.058	16.770
r_o [Ω]	82.682	706.114
	82.434	695.219
	82.711	685.050
	82.522	676.647
	82.221	668.927
$r_{o,avg}$ [Ω]	82.514	686.391
A [m^2]	0.001	0.001
R_o [Ωm]	3.775	31.235
F [-]	15.821	130.911

Table A1: Measured and calculated values used in determining formation factor for Berea Sandstone and Racine Dolomite.

Sample	ϕ_x	Sq. err. – knee vals.	Sq. err. – Lsamp
B_1,w	0.429	2.662×10^{-3}	1.760×10^{-2}
B_1,p	0.429	2.241×10^{-3}	1.747×10^{-2}
B_2,w	0.398	3.284×10^{-7}	6.399×10^{-3}
B_2,p	0.398	1.118×10^{-7}	6.762×10^{-3}
R_1,w	1.000	5.943×10^{-5}	5.696×10^{-2}
R_1,p	1.000	5.943×10^{-7}	5.696×10^{-2}
R_1,w,F	1.000	3.284×10^{-4}	3.152×10^{-4}
R_1,p,F	1.000	3.284×10^{-2}	3.152×10^{-2}

Table A2: Crossover point and error values for each entry for data produced using a pore solid fractal model. Error values defined as point-by-point distance to Lsamp and distance to knee value trend.

Sample	ϕ_x	Sq. err. – knee vals.	Sq. err. – Lsamp
B_1, wash	0.430	1.332×10^{-10}	3.193×10^{-2}
B_1, psf	0.430	1.332×10^{-10}	3.193×10^{-2}
B_2, wash	0.399	1.305×10^{-3}	1.854×10^{-2}
B_2, psf	0.399	1.305×10^{-3}	1.854×10^{-2}
R_1, wash	1.000	1.000×10^{-1}	4.978
R_1, psf	1.000	1.000×10^{-1}	4.978
R_1,w,F	1.000	3.002×10^{-2}	3.002×10^{-4}
R_1,p,F	1.000	2.965×10^{-2}	2.965×10^{-2}

Table A3: Crossover point and error values for each entry for data produced using a pore solid fractal model. Error values defined as point-by-point distance to Lsamp and distance to knee value trend.

	Lower Bound	Upper Bound
p_c	-	1
ϕ_x	-	1
β	ϕ	0.27
D	2.1	2.8
Z	1.75	6
c	0	0.5
Distance to knee vals	0	0.1

Table A4: Evolutionary solver constraints for Berea and Racine samples using a pore solid fractal model for calculation of *V(<r).* Constraint $\phi_x \leq 1$ was omitted for a recalculation of Racine samples.

	Lower Bound	Upper Bound
p_c	-	1
ϕ_x	-	1
α	-2.0	0
Z	1.75	6
c	0	0.5
Distance to knee vals	0	0.1

Table A5: Evolutionary solver constraints for Berea and Racine samples using a truncated power law distribution for calculation of *V(<r).* Constraint $\phi_x \leq 1$ was omitted for a recalculation of Racine samples.

APPENDIX B

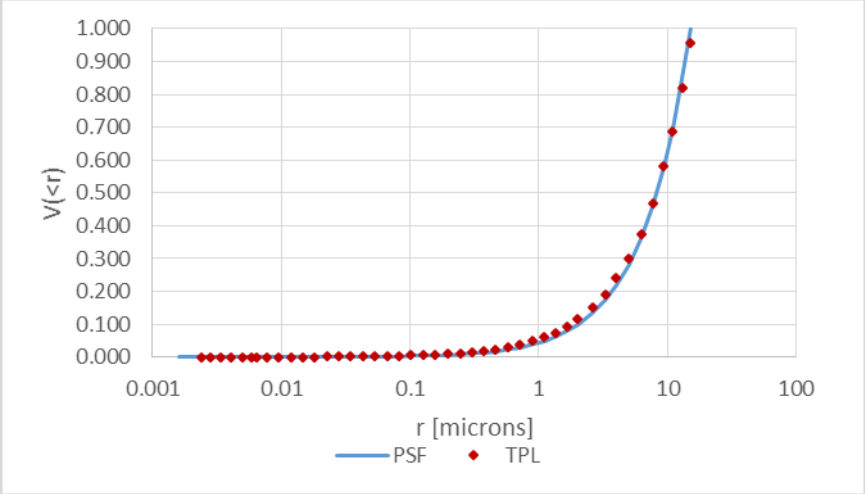

Figure B1: Cumulative probability distribution for Berea_1 created using a Pore Solid Fractal model in blue and a Truncated Power Law distribution in red.

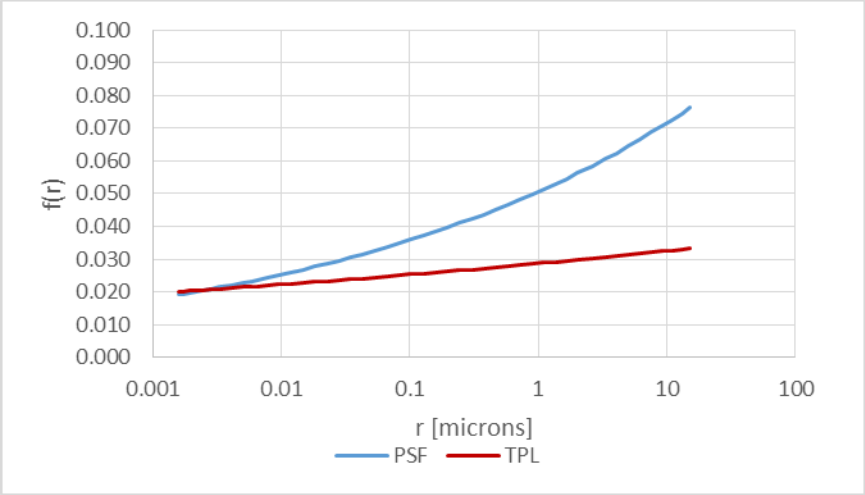

Figure B2: Volumetric probability density for Berea_1 sample created using a Pore Solid Fractal model in blue and a truncated power law distribution in red.

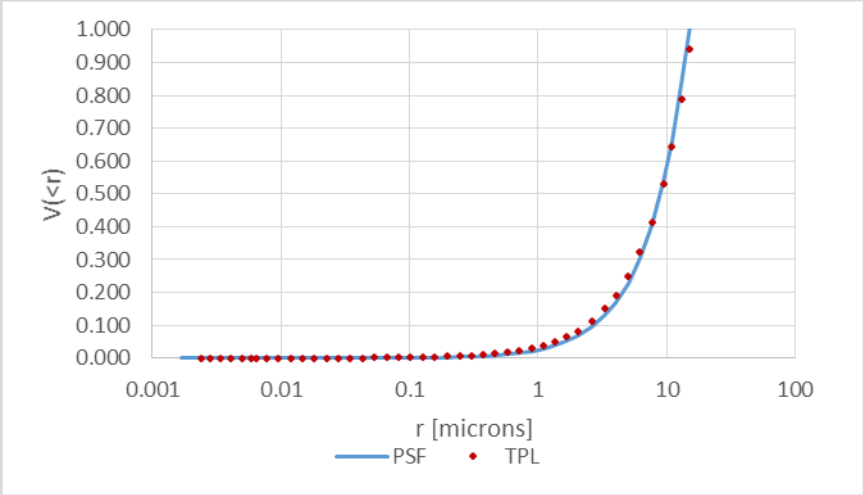

Figure B3: Cumulative probability distribution for Berea_2 created using a Pore Solid Fractal model in blue and a truncated power law distribution in red.

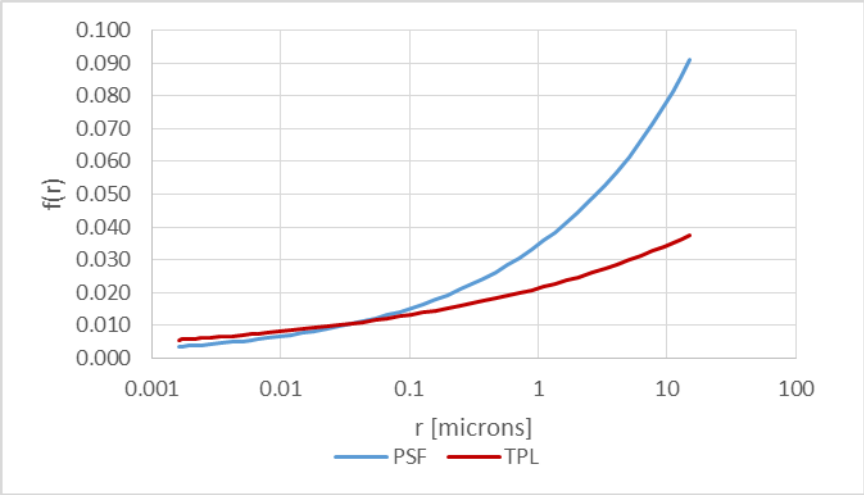

Figure B4: Volumetric probability density for Berea_2 sample created using a Pore Solid Fractal model in blue and a truncated power law distribution in red.

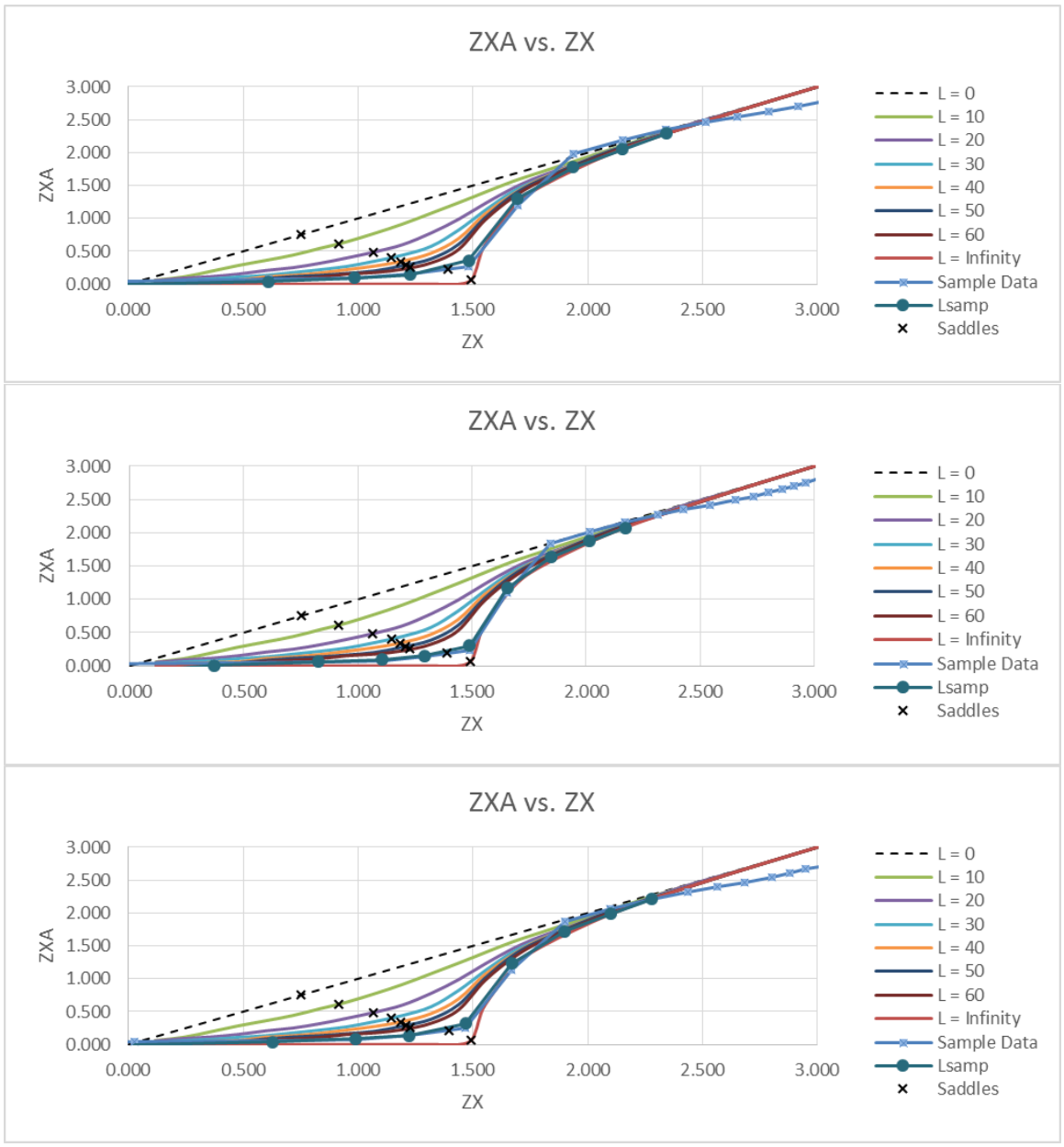

Figure B5: ZXA(r) vs ZX(r) for Berea_1 sample with a rmax value set to 30 µm and solver permeability calculated using (Top) a pore solid fractal model (Eq. 2.23), (Middle) truncated power law distribution (Eq. 2.8), (Bottom) Daigle (2016b) parameters applied to a pore solid fractal model (Eq. 2.23)

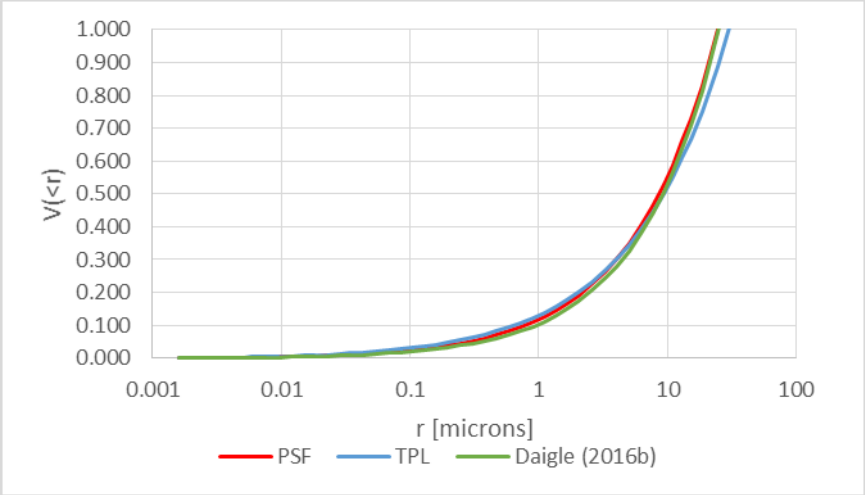

Figure B6: Cumulative probability distribution for Berea_1 created using a Pore Solid Fractal model in blue, a truncated power law distribution in red, and Daigle (2016b) parameters applied to a pore solid fractal model in green.

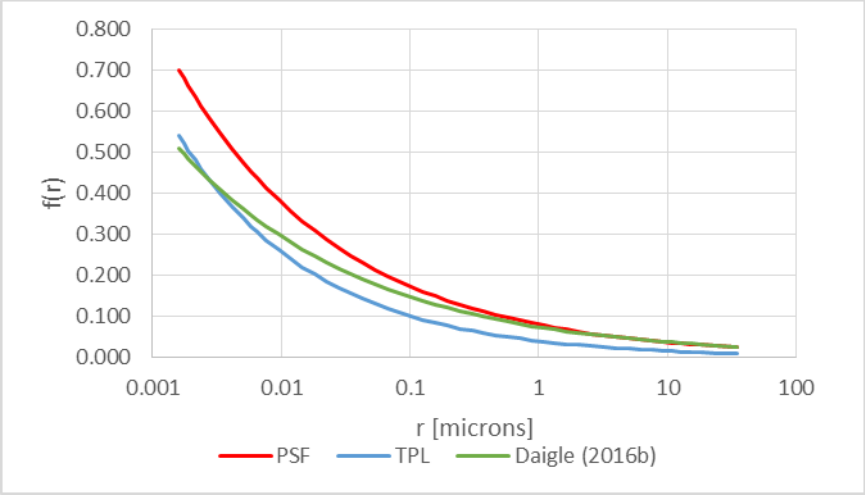

Figure B7: Volumetric probability density for Berea_1 sample created using a Pore Solid Fractal model in blue and a truncated power law distribution in red, and Daigle (2016b) parameters applied to a pore solid fractal model in green.

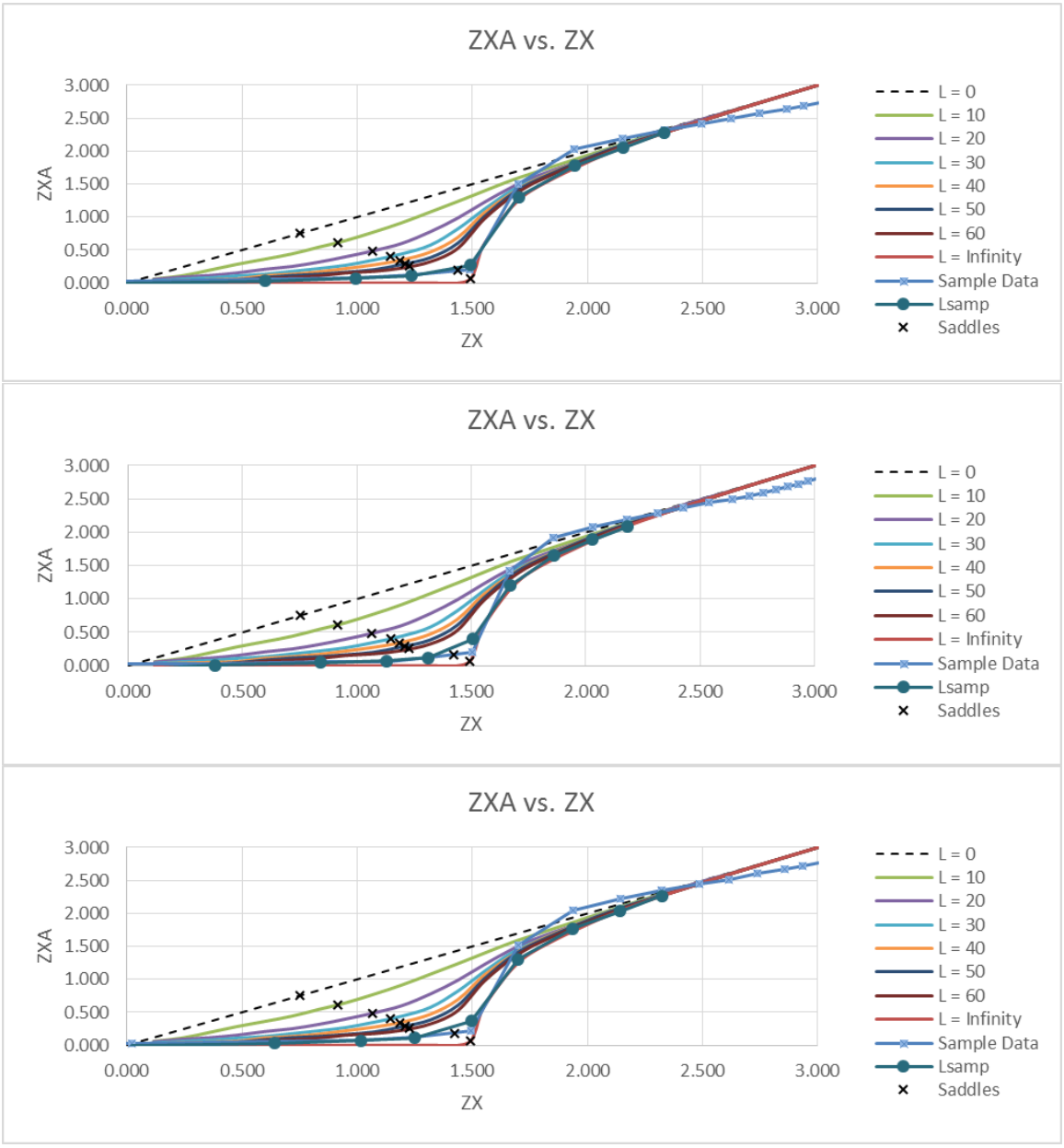

Figure B8: ZXA(r) vs ZX(r) for Berea_2 sample with a rmax value set to 30 µm and solver permeability calculated using (Top) a pore solid fractal model (Eq. 2.23), (Middle) truncated power law distribution (Eq. 2.8), (Bottom) Daigle (2016b) parameters applied to a pore solid fractal model (Eq. 2.23)

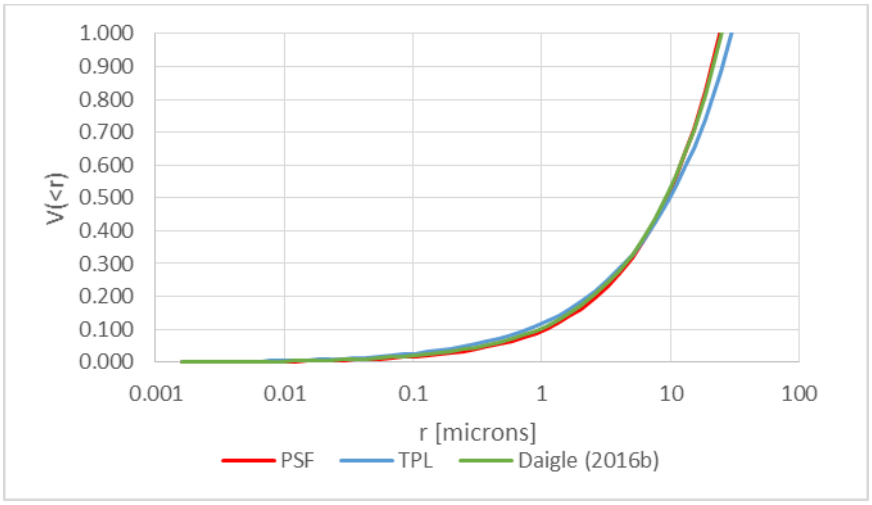

Figure B9: Cumulative probability distribution for Berea_2 created using a Pore Solid Fractal model in blue, a truncated power law distribution in red, and Daigle (2016b) parameters applied to a pore solid fractal model in green.

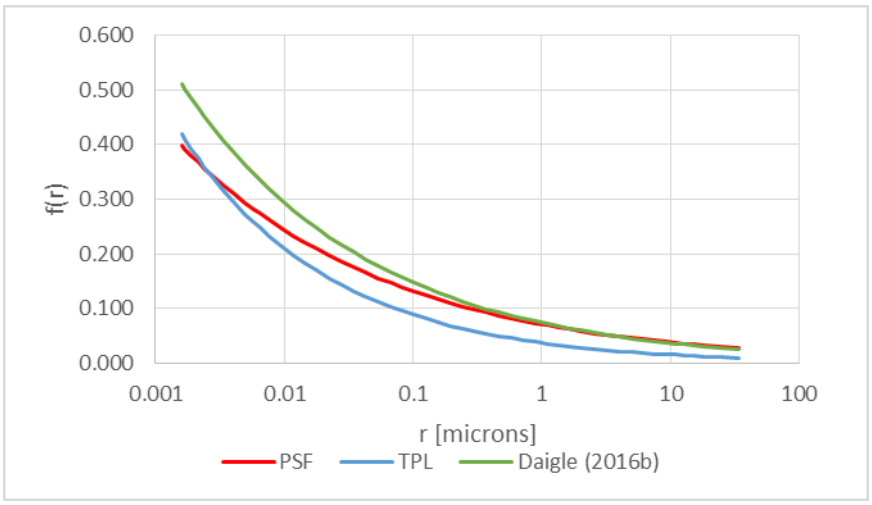

Figure B10: Volumetric probability density for Berea_2 sample created using a Pore Solid Fractal model in blue and a truncated power law distribution in red, and Daigle (2016b) parameters applied to a pore solid fractal model in green.

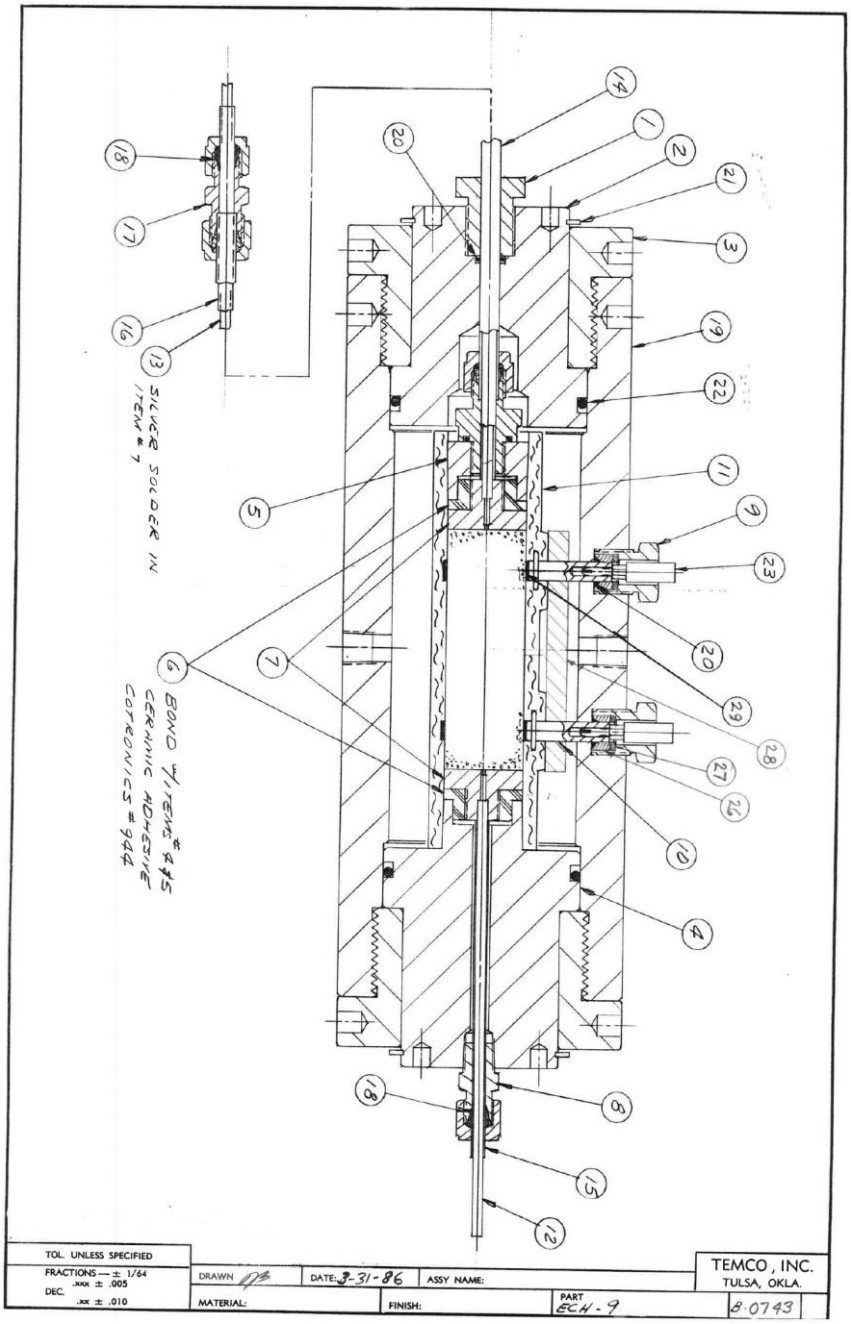

Figure B11: Schematic of the Temco ECH-9 Resistivity Core Holder

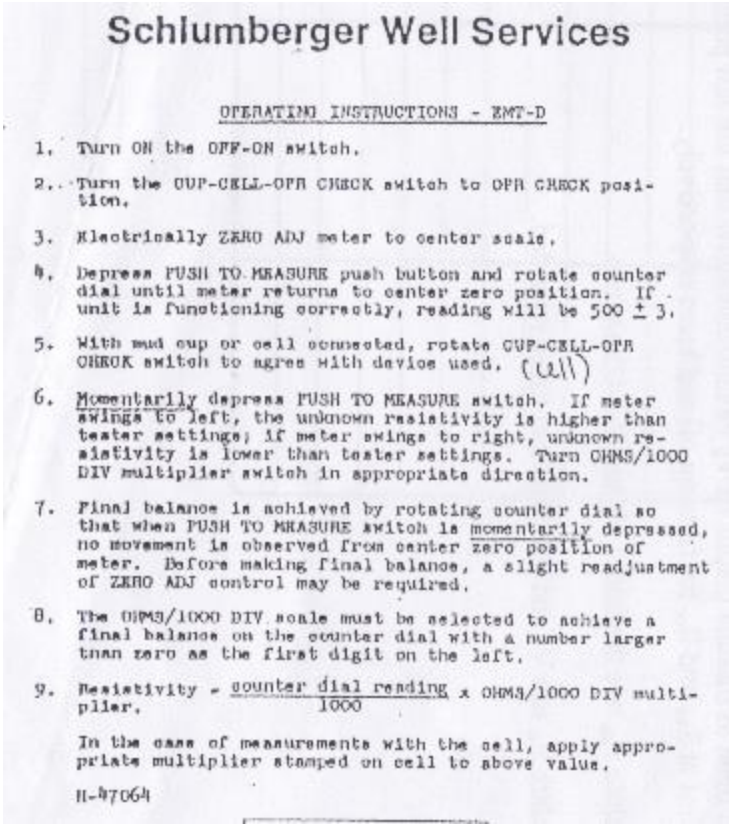

Schlumberger Well Services

OPERATING INSTRUCTIONS - EMT-D

1. Turn ON the OFF-ON switch.

2. Turn the CUP-CELL-OFF CHECK switch to OFF CHECK position.

3. Electrically ZERO ADJ meter to center scale.

4. Depress PUSH TO MEASURE push button and rotate counter dial until meter returns to center zero position. If unit is functioning correctly, reading will be 500 ± 3.

5. With mud cup or cell connected, rotate CUP-CELL-OFF CHECK switch to agree with device used. (CELL)

6. Momentarily depress PUSH TO MEASURE switch. If meter swings to left, the unknown resistivity is higher than tester settings; if meter swings to right, unknown resistivity is lower than tester settings. Turn OHMS/1000 DIV multiplier switch in appropriate direction.

7. Final balance is achieved by rotating counter dial so that when PUSH TO MEASURE switch is momentarily depressed, no movement is observed from center zero position of meter. Before making final balance, a slight readjustment of ZERO ADJ control may be required.

8. The OHMS/1000 DIV scale must be selected to achieve a final balance on the counter dial with a number larger than zero as the first digit on the left.

9. Resistivity = $\frac{\text{counter dial reading}}{1000}$ x OHMS/1000 DIV multiplier.

   In the case of measurements with the cell, apply appropriate multiplier stamped on cell to above value.

H-47064

Figure B12: Operating instructions for Schlumberger water resistivity testing apparatus

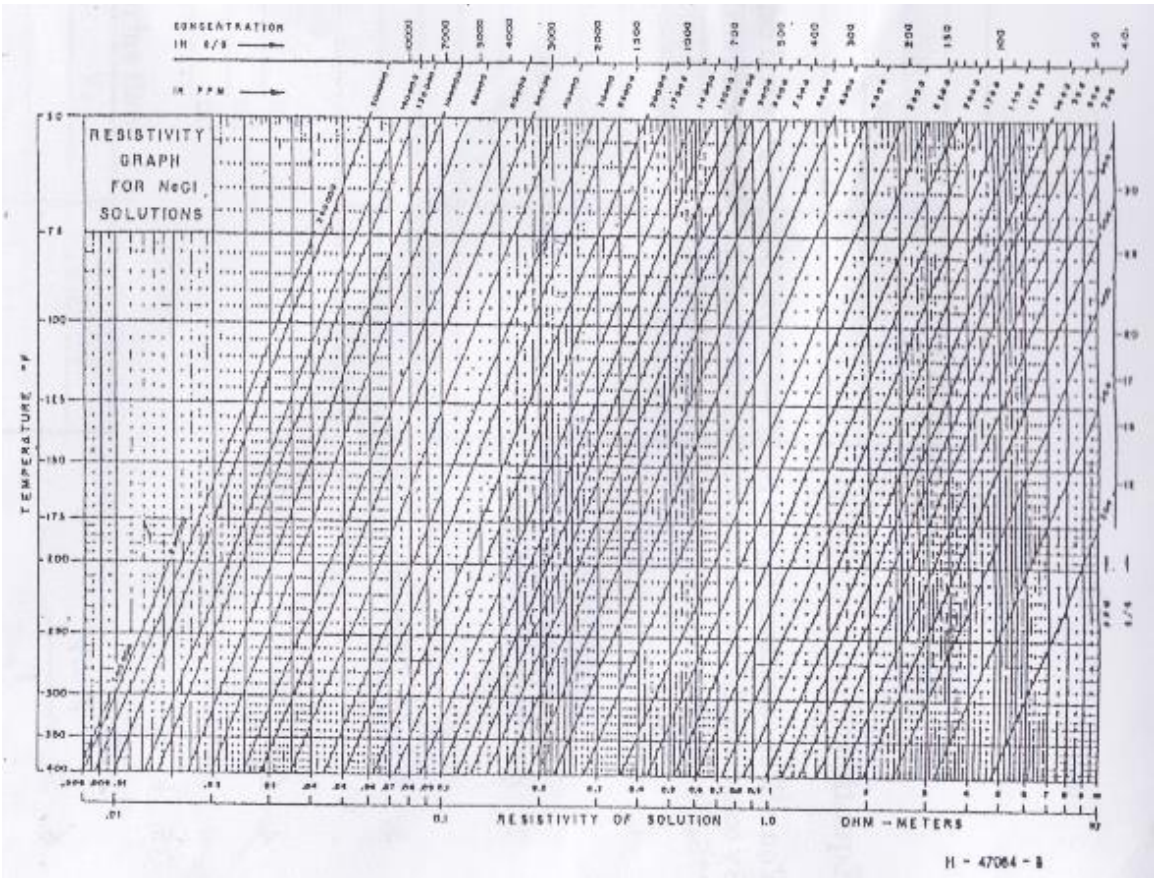

Figure B13: Resistivity graph for NaCl solutions based on temperature and concentration of NaCl

REFERENCES

Archie, G. E. (1942). The Electrical Resistivity Log as an Aid in Determining Some Reservoir Characteristics. *Petroleum Technology*, (October), 54–62. http://doi.org/10.2118/942054-G

Bird, N. R. A., Perrier, E., & Rieu, M. (2000). The water retention function for a model of soil structure with pore and solid fractal distributions. *European Journal of Soil Science*, *51*(1), 55–63. http://doi.org/10.1046/j.1365-2389.2000.00278.x

Broadbent, S. R., & Hammersley, J. M. (1957). Percolation processes. *Mathematical Proceedings of the Cambridge Philosophical Society*, *53*(03), 642. http://doi.org/10.1017/S0305004100032692

Comisky, J. T., Newsham, K. E., Rushing, J. a., & Blasingame, T. a. (2007). A comparative study of capillary-pressure-based empirical models for estimating absolute permeability in tight gas sands. *Proceedings of SPE Annual Technical Conference and Exhibition*, SPE 110050. http://doi.org/10.2118/110050-MS

Daigle, H. (2016a). *Application of critical path analysis for permeability prediction in natural porous media* (Advances in Water Resources Submission). Austin.

Daigle, H. (2016b). Relative permeability to water or gas in the presence of hydrates in porous media from critical path analysis. *Journal of Petroleum Science and Engineering*. http://doi.org/10.1016/j.petrol.2016.07.011

Daigle, H., Ghanbarian, B., Henry, P., & Conin, M. (2015). Universal Scaling of the formation factor in clays: Example from the Nankai Trough. *Journal of Geophysical Research: Solid Earth*, 7361–7375. http://doi.org/10.1002/2015JB012262.Received

Daigle, H., & Johnson, A. (2016). Combining Mercury Intrusion and Nuclear Magnetic Resonance Measurements Using Percolation Theory. *Transport in Porous Media*, *111*(3), 669–679. http://doi.org/10.1007/s11242-015-0619-1

Friedman, S. P., & Seaton, N. A. (1998). Critical path analysis of the relationship between permeability and electrical conductivity of three-dimensional pore networks. *Water Resources Research*, *24*(5), 681–693. http://doi.org/10.1029/98WR00939

Ghanbarian, B., Hunt, A. G., Ewing, R. P., & Skinner, T. E. (2014). Universal scaling of the formation factor in porous media derived by combining percolation and effective medium theories. *Geophysical Research Letters*, *41*(11), 3884–3890. http://doi.org/10.1002/2014GL060180

Hunt, A. G. (1998). Upscaling in Subsurface Transport Using Cluster Statistics of Percolation. *Transport in Porous Media*, *30*(2), 177–198. http://doi.org/10.1023/A:1006534922791

Hunt, A. G. (2001). Applications of percolation theory to porous media with distributed local conductances. *Advances in Water Resources*, *24*(3-4), 279–307. http://doi.org/10.1016/S0309-1708(00)00058-0

Katz, A. J., & Thompson, A. H. (1986). *Quantitative Prediction of Permeability and Electrical Conductivity in Porous Rock*. Retrieved from http://dx.doi.org/10.1103/PhysRevB.34.8179

Katz, A. J., & Thompson, A. H. (1987). Prediction of Rock Electrical Conductivity From Mercury Injection Measurements Or / Or, *92*(6), 599–607. http://doi.org/10.1029/JB092iB01p00599

Le Doussal, P. (1989a). Percolation like exponent for the conductivity of highly disordered resistor networks. *Physical Review B*, *39*(1), 881–884. http://doi.org/10.1103/PhysRevB.39.881

Le Doussal, P. (1989b). Permeability versus conductivity for porous media with wide distribution of pore sizes. *Physical Review B*, *39*(7), 4816–4819. http://doi.org/10.1103/PhysRevB.39.4816

Liu, H., Zhang, L., & Seaton, N. A. (1992). Determination of the connectivity of porous solids from nitrogen sorption measurements - II. Generalisation. *Chemical Engineering Science*, *47*(17-18), 4393–4404. http://doi.org/10.1016/0009-2509(92)85117-T

Liu, H., Zhang, L., & Seaton, N. A. (1993). Analysis of Sorption Hysteresis in Mesoporous Solids Using a Pore Network Model. *Journal of Colloid and Interface Science*. http://doi.org/10.1006/jcis.1993.1113

Mishra, B., & Sharma, M. (1988). Measurement of pore size distributions from capillary pressure curves. *AIChE Journal*. http://doi.org/10.1002/aic.690340420

P.C. Carman. (1956). *Flow of Gases Through Porous Media*. New York: Academic Press Inc., Publishers. http://doi.org/10.1016/0010-2180(57)90038-X

Perrier, E., Bird, N., & Rieu, M. (1999). Generalizing the fractal model of soil structure: the pore- solid fractal approach. *Geoderma*, *88*(3-4), 137–164. Retrieved from ISI:000079107800004

Purcell, W. R. (1949). Capillary Pressures - Their Measurement Using Mercury and the Calculation of Permeability Therefrom. *Journal of Petroleum Technology*, *1*(2), 1949. http://doi.org/10.2118/949039-G

Sahimi, M. (1993). Flow Phenomena in Rocks - from Continuum Models to Fractals, Percolation, Cellular-Automata, and Simulated Annealing. *Reviews of Modern Physics*, *65*(4), 1393–1534. http://doi.org/10.1103/RevModPhys.65.1393

Seaton, N. A. (1991). Determination of the connectivity of porous solids from nitrogen sorption measurements. *Chemical Engineering Science*, *46*(8), 1895–1909.

Skaggs, T. H. (2003). Effects of finite system-size and finite inhomogeneity on the conductivity of broadly distributed resistor networks. *Physica B: Condensed Matter*, *338*(1-4), 266–269. http://doi.org/10.1016/j.physb.2003.08.005

Skaggs, T. H. (2011). Assessment of critical path analyses of the relationship between permeability and electrical conductivity of pore networks. *Advances in Water Resources*, *34*(10), 1335–1342. http://doi.org/10.1016/j.advwatres.2011.06.010

Tyč, S., & Halperin, B. I. (1989). Random resistor network with an exponentially wide distribution of bond conductances. *Physical Review B*, *39*(1), 877–880. http://doi.org/10.1103/PhysRevB.39.877

VITA

Derek Andrews Tinker graduated with a Master of Science in Engineering from The University of Texas at Austin. His research focused on verifying new findings about the fundamental length scales that describe transport through porous media using laboratory testing on core samples. He then defined a possible method for finite scaling correction and permeability prediction by utilizing mercury intrusion capillary pressure data constrained to match type curves of accessibility functions to define parameterization values for core samples of specific lithologies without the need for an independent pore size distribution measurement.

Permanent email: tinker.derek@gmail.com

This thesis was typed by the author.